A NONLINEAR UNIFIED STATE-SPACE MODEL FOR SHIP MANEUVERING AND CONTROL IN A SEAWAY

THOR I. FOSSEN
Department of Engineering Cybernetics
Norwegian University of Science and Technology
NO-7491 Trondheim, Norway
E-mail: fossen@ieee.org

This article presents a unified state-space model for ship maneuvering, station-keeping, and control in a seaway. The frequency-dependent potential and viscous damping terms, which in classic theory results in a convolution integral not suited for real-time simulation, is compactly represented by using a state-space formulation. The separation of the vessel model into a low-frequency model (represented by zero-frequency added mass and damping) and a wave-frequency model (represented by motion transfer functions or RAOs), which is commonly used for simulation, is hence made superfluous.

Keywords: ship modelling, equations of motion, hydrodynamics, maneuvering, seakeeping, autopilots, dynamic positioning.

1 Introduction

Motivated by the work of Bishop and Price [1981] and Bailey *et al.* [1998], a unified state-space model for ship maneuvering, station-keeping, and control in a seaway is derived. The dynamic equations of motion for a ship exposed to waves have evolved from two main directions:

- *Maneuvering theory*
- *Seakeeping theory*

In maneuvering theory it is common to assume that the ship is moving in restricted calm water, e.g. in sheltered waters or in a harbor. Hence, the ship model is derived for a ship moving at positive speed U under a zero-frequency assumption such that added mass and damping can be represented by using hydrodynamic derivatives. Seakeeping analysis is used in operability calculations to obtain operability diagrams according to the adopted criteria. It also refers to the motions of a vessel in waves usually at a specific speed (included station-keeping, i.e. zero speed) and heading in a sinusoidal, irregular or random seaway. This includes analyses of motions in the time-domain for frequency-dependent added mass and damping.

It is desirable to unify these theories such that the ship motions can be described more accurately for different speeds, sea states, and operations. This should be done in the time-domain in order to facilitate performance tests and design of feedback control systems. Another application is real-time training simulators. For this purpose we will discuss a:

- *Unified time-domain theory for maneuvering and seakeeping*

where it is possible to include systems for feedback control, that is autopilots, dynamic positioning systems, roll damping systems etc.

The unified model will be derived using a state-space approach since this is the standard representation used in feedback control systems.

The kinematic and dynamic equations of motion for ships are presented using principles from the classical maneuvering and seakeeping theories. The relationship between frequency-dependent *oscillatory derivatives*, *hydrodynamic derivatives*, and frequency dependent *hydrodynamic coefficients* are explained through examples. The final unified model is represented in the time-domain as a 6 degree-of-freedom (DOF) nonlinear state-space model. The state-space model is written in a compact matrix-vector setting such that structural properties like symmetry, skew-symmetry, positive definiteness, passivity etc. can be exploited when designing control systems.

The state-space models are used as basis for development of 3 DOF (surge, sway, and yaw) nonlinear dynamic positioning systems for station-keeping and low-speed maneuvering of ships and rigs. Autopilot design in 1 DOF for ships moving at moderate speed is also discussed. The model parameters for floating vessels can be computed using commercial 2D potential theory programs. The details regarding this are presented in the case study

Feedback control systems design for ships goes back to the invention of the North-seeking gyroscope in 1908

by Anschutz, the ballistic gyroscope in 1911 by Sperry [Allensworth, 1999], and the analysis of the three-term PID-controller [Minorsky, 1922]. These developments were fundamental for the evolution of modern model-based ship control systems for station-keeping and maneuvering. More recently, the development of global satellite navigation systems and inertial measurements technology have further contributed to the design of highly sophisticated nonlinear model-based ship control systems. From a historical point of view, the PID-controller was the dominating design technique until the invention of the Kalman filter and the linear quadratic optimal controller (LQG) in the 1960s.

Motivated by this Balchen *et al.* [1976] proposed to model the wave-induced disturbances as 2nd-order oscillators in the Kalman estimator in order to filter out 1st-order wave-induced disturbances from the feedback loop. This technique is today known as *wave filtering,* and it replaced the notch filter in dynamic positioning (DP) systems and autopilots. The concept of wave filtering has further been refined by using linear $\mathcal{H}$-infinity controllers with frequency-dependent weighting. This allows the designer to put penalties on the wave-induced disturbances in a limited frequency range. Nonlinear ship control systems became popular in the 1990s using Lyapunov methods for stability analyses [Fossen, 1994, 2002].

2 Notation and Other Preliminaries

The notation used in this paper complies with SNAME [1950], see Table 1.

Table 1: The notation of SNAME (1950) for marine vessels

DOF		force/ moment	linear/angular velocity	positions/ Euler angles
1	surge	X	u	x
2	sway	Y	v	y
3	heave	Z	w	z
4	roll	K	p	ϕ
5	pitch	M	q	θ
6	yaw	N	r	ψ

2.1 Degrees of Freedom

In maneuvering, a marine vessel experiences motion in 6 *degrees-of-freedom* (DOF). The motion in the horizontal plane is referred to as *surge* (longitudinal motion, usually superimposed on the steady propulsive motion) and *sway* (sideways motion). Heading, or *yaw* (rotation about the vertical axis) describes the course of the vessel. The remaining three DOFs are *roll* (rotation about the longitudinal axis), *pitch* (rotation about the transverse axis), and *heave* (vertical motion), see Figure 1.

Roll is probably the most troublesome DOF, since it produces the highest accelerations and, hence, is the principal villain in seasickness. Similarly, pitching and heaving feel uncomfortable to humans. When designing ship autopilots, yaw is the primary mode for feedback control.

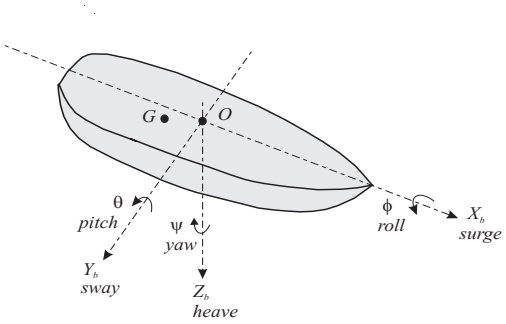

Figure 1: Definitions of ship motions in the *b*-frame.

2.2 Generalized Position, Velocity and Force

The generalized position, velocity, and force vectors are defined according to Fossen [1994, 2002]:

$$\boldsymbol{\eta} = [n, e, d, \phi, \theta, \psi]^\top \in \mathbb{R}^3 \times \mathcal{S}^3 \quad (1)$$

$$\boldsymbol{\nu} = [u, v, w, p, q, r]^\top \in \mathbb{R}^6 \quad (2)$$

$$\boldsymbol{\tau} = [X, Y, Z, K, M, N]^\top \in \mathbb{R}^6 \quad (3)$$

where the Euler angles can be be conveniently represented by the vector:

$$\boldsymbol{\Theta} = [\phi, \theta, \psi]^\top \in \mathcal{S}^3 \quad (4)$$

The North-East-Down position vector is denoted as

$$\mathbf{p} = [n, e, d]^\top \in \mathbb{R}^3 \quad (5)$$

The *Euclidean space* of dimension n is denoted $\mathbb{R}^n$ while $\mathcal{S}^2$ denotes a *torus* of dimension 2 (shape of a donut) implying that there are two angles defined on the interval $[0, 2\pi]$. In the 3-dimensional case the set is denoted as $\mathcal{S}^3$.

2.3 Oscillatory and Hydrodynamic Derivatives

The frequency-dependent *oscillatory derivatives* are written as [Bailey *et al.*, 1998]:

$$F_\beta(\omega) \ - \text{oscillatory derivative} \quad (6)$$

where F is the generalized force, β is the motion component:

$$F \in \{X, Y, Z, K, M, N\}$$

$$\beta \in \{\dot{u}, \dot{v}, \dot{w}, \dot{p}, \dot{q}, \dot{r}, u, v, w, p, q, r, x, y, z, \phi, \theta, \psi\}$$

and ω is the frequency of oscillation. Examples of oscillatory derivatives are:

$$\tilde{Y}_v(\omega), \ \tilde{N}_r(\omega), \ \tilde{K}_{\dot{p}}(\omega), \text{etc.} \quad (7)$$

These derivatives are frequency dependent and they can be derived from maneuvering based PMM experiments [Gertler, 1959], [Chislett and Strøm-Tejsen, 1965].

The limiting value for $\omega = 0$ is defined as the *hydrodynamic derivative*, that is*:*

$$F_\beta \triangleq \frac{\partial F}{\partial \beta} \triangleq \tilde{F}_\beta(0) \ - \text{hydrodynamic derivative} \tag{8}$$

For instance, the hydrodynamic derivative $Y_{\dot{w}}$ corresponds to a force Y in the y-direction due to an acceleration $\dot{w}$ in the z-direction, while the hydrodynamic derivative K_p corresponds to the moment K due to an angular velocity p about the x-axis. This suggests [SNAME, 1950]:

$$Y_{\dot{w}} \triangleq \frac{\partial Y}{\partial \dot{w}}, \qquad K_p \triangleq \frac{\partial K}{\partial p} \tag{9}$$

The resulting force and moment are then:

$$Y = Y_{\dot{w}}\dot{w}, \qquad K = K_p p \tag{10}$$

The 6 DOF generalized mass and damping matrices in terms of *oscillatory derivatives* are denoted as $\tilde{\mathbf{M}}_A(\omega)$ and $\tilde{\mathbf{D}}(\omega)$, while the matrices:

$$\mathbf{M}_A \triangleq \tilde{\mathbf{M}}_A(0) \tag{11}$$

$$\mathbf{D} \triangleq \tilde{\mathbf{D}}(0) \tag{12}$$

for the slow motion *hydrodynamic derivatives* take the following form [Fossen, 1994, 2002]:

$$\mathbf{M}_A = -\begin{bmatrix} X_{\dot{u}} & X_{\dot{v}} & X_{\dot{w}} & X_{\dot{p}} & X_{\dot{q}} & X_{\dot{r}} \\ Y_{\dot{u}} & Y_{\dot{v}} & Y_{\dot{w}} & Y_{\dot{p}} & Y_{\dot{q}} & Y_{\dot{r}} \\ Z_{\dot{u}} & Z_{\dot{v}} & Z_{\dot{w}} & Z_{\dot{p}} & Z_{\dot{q}} & Z_{\dot{r}} \\ K_{\dot{u}} & K_{\dot{v}} & K_{\dot{w}} & K_{\dot{p}} & K_{\dot{q}} & K_{\dot{r}} \\ M_{\dot{u}} & M_{\dot{v}} & M_{\dot{w}} & M_{\dot{p}} & M_{\dot{q}} & M_{\dot{r}} \\ N_{\dot{u}} & N_{\dot{v}} & N_{\dot{w}} & N_{\dot{p}} & N_{\dot{q}} & N_{\dot{r}} \end{bmatrix} \tag{13}$$

$$\mathbf{D} = -\begin{bmatrix} X_u & X_v & X_w & X_p & X_q & X_r \\ Y_u & Y_v & Y_w & Y_p & Y_q & Y_r \\ Z_u & Z_v & Z_w & Z_p & Z_q & Z_r \\ K_u & K_v & K_w & K_p & K_q & K_r \\ M_u & M_v & M_w & M_p & M_q & M_r \\ N_u & N_{vp} & N_w & N_p & N_q & N_r \end{bmatrix} \tag{14}$$

Notice that the matrices are multiplied with -1 such that $\mathbf{M}_A > 0$ and $\mathbf{D} > 0$ (positive mass and damping).

2.4 Generalized Rigid-Body Inertia Matrix

The generalized rigid-body inertia matrix is defined as [Fossen, 1994, 2002]:

$$\mathbf{M}_{RB} = \begin{bmatrix} m\mathbf{I}_{3\times 3} & -m\mathbf{S}(\mathbf{r}_g^b) \\ m\mathbf{S}(\mathbf{r}_g^b) & \mathbf{I}_o \end{bmatrix}$$

$$= \begin{bmatrix} m & 0 & 0 & 0 & mz_g & -my_g \\ 0 & m & 0 & -mz_g & 0 & mx_g \\ 0 & 0 & m & my_g & -mx_g & 0 \\ 0 & -mz_g & my_g & I_x & -I_{xy} & -I_{xz} \\ mz_g & 0 & -mx_g & -I_{yx} & I_y & -I_{yz} \\ -my_g & mx_g & 0 & -I_{zx} & -I_{zy} & I_z \end{bmatrix}$$

where m is the mass, $\mathbf{I}_{3\times 3} \in \mathbb{R}^{3\times 3}$ is the identity matrix, $\mathbf{r}_g^b = [x_g, y_g, z_g]^\top$ are the coordinates to the center of gravity with respect to the point O in the body-fixed reference frame, and:

$$\mathbf{I}_o = \begin{bmatrix} I_x & -I_{xy} & -I_{xz} \\ -I_{yx} & I_y & -I_{yz} \\ -I_{zx} & -I_{zy} & I_z \end{bmatrix} \tag{15}$$

is the inertia tensor. For notational simplicity the vector cross product:

$$\mathbf{a} \times \mathbf{b} = \mathbf{S}(\mathbf{a})\mathbf{b} \tag{16}$$

is written in terms of a skew-symmetric matrix $\mathbf{S} \in SS(3)$ defined as:

$$\mathbf{S}(\boldsymbol{\lambda}) = -\mathbf{S}^\top(\boldsymbol{\lambda}) = \begin{bmatrix} 0 & -\lambda_3 & \lambda_2 \\ \lambda_3 & 0 & -\lambda_1 \\ -\lambda_2 & \lambda_1 & 0 \end{bmatrix} \quad \boldsymbol{\lambda} = \begin{bmatrix} \lambda_1 \\ \lambda_2 \\ \lambda_3 \end{bmatrix} \tag{17}$$

2.5 Rotation Matrices

The notation $\mathbf{R}_a^b \in SO(3)$ implies that the rotation matrix $\mathbf{R}_a^b$ between two frames a and b (from b to a) is an element in $SO(3)$, that is the *special orthogonal group of order 3:*

$$SO(3) = \left\{\mathbf{R}_a^b | \mathbf{R}_a^b \in \mathbb{R}^{3\times 3},\ \mathbf{R}_a^b \text{ is orthogonal, } \det \mathbf{R}_a^b = 1\right\}$$

The group $SO(3)$ is a subset of all *orthogonal matrices of order 3*, i.e. $SO(3) \subset O(3)$ where $O(3)$ is defined as:

$$O(3) = \left\{\mathbf{R}_a^b | \mathbf{R}_a^b \in \mathbb{R}^{3\times 3}, \quad \mathbf{R}_a^b (\mathbf{R}_a^b)^\top = (\mathbf{R}_a^b)^\top \mathbf{R}_a^b = \mathbf{I}\right\}$$

Hence it follows that

$$(\mathbf{R}_a^b)^{-1} = (\mathbf{R}_a^b)^\top = \mathbf{R}_b^a$$

A principal rotation α about the i-axis is denoted as $R_{i,\alpha}$. The principal rotations (one axis rotations) about the $x, y,$

and z-axes are defined as [Fossen, 2002]:

$$\mathbf{R}_{x,\phi} = \begin{bmatrix} 1 & 0 & 0 \\ 0 & \mathrm{c}\phi & -\mathrm{s}\phi \\ 0 & \mathrm{s}\phi & \mathrm{c}\phi \end{bmatrix} \quad (18)$$

$$\mathbf{R}_{y,\theta} = \begin{bmatrix} \mathrm{c}\theta & 0 & \mathrm{s}\theta \\ 0 & 1 & 0 \\ -\mathrm{s}\theta & 0 & \mathrm{c}\theta \end{bmatrix} \quad (19)$$

$$\mathbf{R}_{z,\psi} = \begin{bmatrix} \mathrm{c}\psi & -\mathrm{s}\psi & 0 \\ \mathrm{s}\psi & \mathrm{c}\psi & 0 \\ 0 & 0 & 1 \end{bmatrix} \quad (20)$$

where $\mathrm{s}\cdot = \sin(\cdot)$, $\mathrm{c}\cdot = \cos(\cdot)$, while ϕ, θ, and ψ are the *Euler angles.*

3 Maneuvering and Seakeeping – A Motivating Example

Consider a ship moving in sway (mass-damper) and assume that the other modes can be neglected. This can be mathematically described by considering the motion in one degree of freedom [Faltinsen, 1990], [Newman, 1977]:

$$\dot{y} = v \quad (21)$$

$$[m + A_{22}(\omega)]\,\dot{v} + B_{22}(\omega)v = \tau_{2,\text{FK+diff}} + \tau_2 \quad (22)$$

where y is the sway position, v is the velocity and:

m	= mass
$A_{22}(\omega)$	= frequency-dependent added mass
$B_{22}(\omega)$	= frequency-dependent damping
$\tau_{2,\text{FK+diff}}$	= Froude-Krylov and diffraction force in sway
τ_2	= control force in sway
ω	= frequency of forced oscillation

Notice that the hydrodynamic *added mass* and *damping* coefficients, $A_{22}(\omega) = -\tilde{Y}_{\dot{v}}(\omega)$ and $B_{22}(\omega) = -\tilde{Y}_{v}(\omega)$, depend on the frequency of the forced oscillation, see Figure 2. The wave excitation force $\tau_{2,\text{FK+diff}}$ is due to wave diffraction whereas the mass and damping forces, $A_{22}(\omega)\dot{v}$ and $B_{22}(\omega)v$, are caused by the hydrodynamic reaction as a result of the movement of the ship in the water.

The water is assumed to be ideal and thus potential theory can be applied. We will denote frequency-dependent potential damping in sway as $B_{22p}(\omega)$ and frequency-dependent damping due to viscous effects, e.g. skin friction and pressure loads, as $B_{22v}(\omega)$. This suggests that the total frequency-dependent linear damping coefficient is:

$$B_{22}(\omega) = B_{22p}(\omega) + B_{22v}(\omega) \quad (23)$$

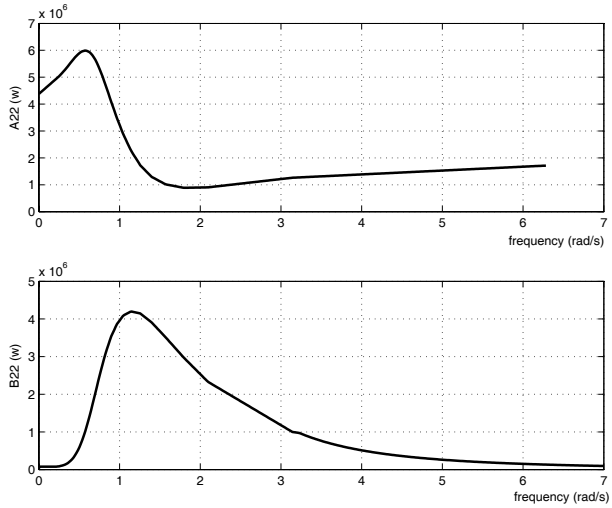

Figure 2: Hydrodynamic added mass $A_{22}(\omega)$ and potential damping $B_{22p}(\omega)$ as a function of frequency ω for zero velocity $u = 0$.

The *potential coefficients* or *hydrodynamic coefficients* $A_{22}(\omega)$ and $B_{22p}(\omega)$ are usually computed using hydrodynamic software, whereas the viscous part $B_{22v}(\omega)$ is more complicated to determine. Note that $B_{22p}(0) = 0$.

An experimentally motivated model is to assign a nonzero value for $\omega = 0$ which is decaying as ω increases. In Bailey *et al.* [1998] a ramp function was used for this purpose. The viscous damper is here modelled as an exponentially decaying function:

$$B_{22v}(\omega) = \beta_{22} e^{-\alpha\omega}, \qquad \alpha > 0 \quad (24)$$

where β_{22} is the zero frequency damping coefficient, that is $B_{22v}(0) = \beta_{22}$. The exponential function has excellent numerical properties and it is straightforward to transform the frequency-dependent model to the time domain.

Maneuvering Theory (Low-Frequency Model)

For a ship maneuvering in calm water, $\omega = 0$, the effect due to 1st-order wave loads $\tau_{2,\text{FK+diff}}$ is removed from (21)–(22), such that the *low-frequency* (LF) model becomes:

$$\dot{y}_{LF} = v_{LF} \quad (25)$$

$$(m - Y_{\dot{v}})\dot{v}_{LF} - Y_v v_{LF} = \tau_2 \quad (26)$$

where v_{LF} and y_{LF} are the LF velocity and position in sway, respectively. The assumption that the 1st-order wave-induced force $\tau_{2,\text{FK+diff}}$ is zero is justified in Section 3.1 using linear superposition.

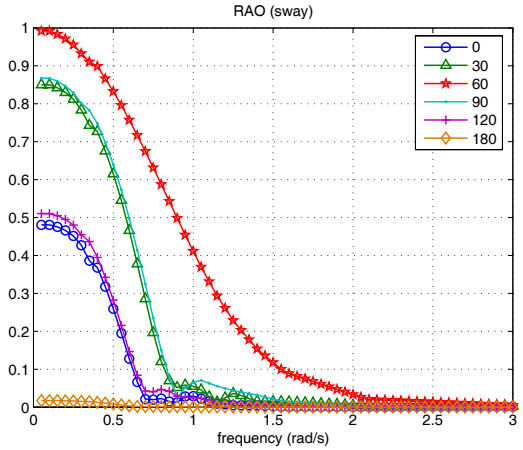

Figure 3: RAOs as a function of wave direction $0 - 180$ (deg) and frequency ω (rad/s).

The *hydrodynamic (slow motion) derivatives* are defined in terms of zero-frequency *hydrodynamic coefficients*:

$$-Y_{\dot{v}} \triangleq A_{22}(0) \tag{27}$$

$$-Y_{v} \triangleq B_{22}(0) = B_{22v}(0) = \beta_{22} \tag{28}$$

The hydrodynamic derivatives Y_v and $Y_{\dot{v}}$ are usually computed from experimental data using curve fitting and system identification techniques. The frequency-dependent hydrodynamic coefficients $A_{22}(\omega)$ and $B_{22}(\omega)$ can also be computed using hydrodynamic potential theory programs or be determined from a PMM experiment where a scale model of the ship is oscillated at different frequencies ω and the resulting hydrodynamic force is measured [Lewis, 1989].

Seakeeping Theory (Models for Wave Loads)

The drawback with the model (25)–(26) is that only the LF part of the hydrodynamic forces is included in the dynamic model of the ship while the 1st-order *wave-frequency* (WF) motions $\tau_{2,\text{FK+diff}}$ must be added by assuming linear superposition.

The WF motions can be computed using motion transfer functions which are defined as the response amplitude per unit wave amplitude. This is also referred to as the *Response Amplitude Operator* (RAO). For our simple model (21)–(22) this corresponds to the ratio between the position amplitude y_{WF} of the oscillating sway position and the wave amplitude ζ_a, given by [Journée and Massie, 2001]:

$$RAO_2(s, \psi_r) = \frac{y_{WF}(s, \psi_r)}{\zeta_a} \tag{29}$$

whereψ_r is the wave direction relative to the ship. Hence, for $s = j\omega$ and:

$$\zeta = \zeta_a \cos(\omega t + \varepsilon) \tag{30}$$

where ε is the wave phase angle, the WF motions in sway become:

$$y_{WF}(t) = \zeta_a \left| RAO_2(j\omega, \psi_r) \right| \cos\left(\omega t + \angle RAO_2(j\omega, \psi_r) + \varepsilon\right) \tag{31}$$

Here $\angle RAO(j\omega, \psi_r)$ denotes the RAO phase angle. For a typical ship, the RAOs in the y-direction are shown in Figure 3. The curves were computed using the strip theory program ShipX (VERES) by Marintek [Fathi, 2004].

An alternative method is to compute the 1st-order wave loads $\tau_{2,\text{FK+diff}}$ in (22) directly using the *force transfer function* (FTF):

$$FTF_2(s, \psi_r) = \frac{\tau_{2,\text{FK+diff}}(s, \psi_r)}{\zeta_a} \tag{32}$$

such that:

$$\begin{aligned} \tau_{2,\text{FK+diff}}(t) \quad &= \quad \zeta_a \left| FTF_2(j\omega, \psi_r) \right| \cdot \\ &\quad \cos\left(\omega t + \angle FTF_2(j\omega, \psi_r) + \varepsilon\right) \end{aligned} \tag{33}$$

3.1 Linear Superposition of Low-Frequency (LF) and Wave-Frequency (WF) Models

The models (25)–(26) and (29) can be combined to describe the 1st-order ship-wave interactions $\tau_{2,\text{FK+diff}}$. The principle of linear superposition [Denis and Pierson, 1953] suggests that (Figure 4):

$$y = y_{LF} + y_{WF} \tag{34}$$

When designing a feedback control system, e.g. an autopilot or a dynamic positioning system, the WF motions are treated as measurement noise that can be added to the LF motions and a disturbance observer (wave filter) is designed to remove the WF from entering the feedback loop, see Figure 5. Moreover, the control system should only compensate for the LF motions in order to reduce wear and tear of the propellers and rudders.

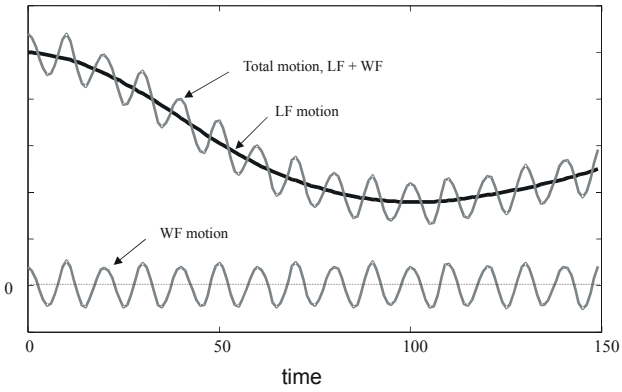

Figure 4: The plot shows how the total motion of a ship can be separated into LF and WF motion components (RAOs).

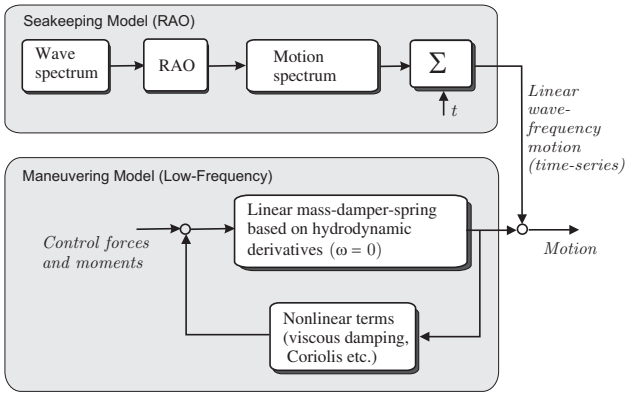

Figure 5: Linear superposition of maneuvering (low-frequency) model and wave frequency model based on RAOs [Perez and Fossen, 2004].

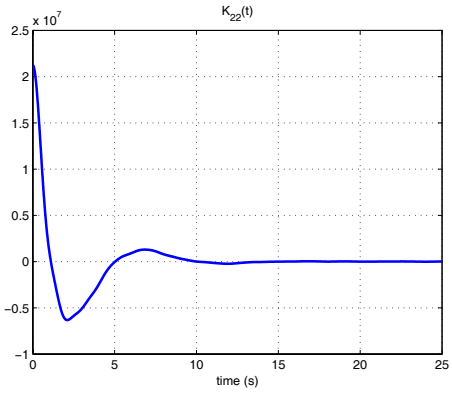

Figure 6: Typical impulse response function $K_{22}(t)$ as a function of time t.

3.2 Frequency-Dependent Model with Wave Loads

The disadvantage with the LF and WF model representations is that hydrodynamic wave loads are represented as zero mean WF motions added to the LF ship motions. This model cannot be used for multi-body operations with interaction forces and it is not possible to monitor the wave-induced forces directly since they are represented as disturbances in position and velocity (motion transfer functions).

From a physical point-of-view, wave loads should be modelled as forces acting on the ship through Newton's law. This can be done using the frequency-dependent vessel model (22) which is valid for different sea states.

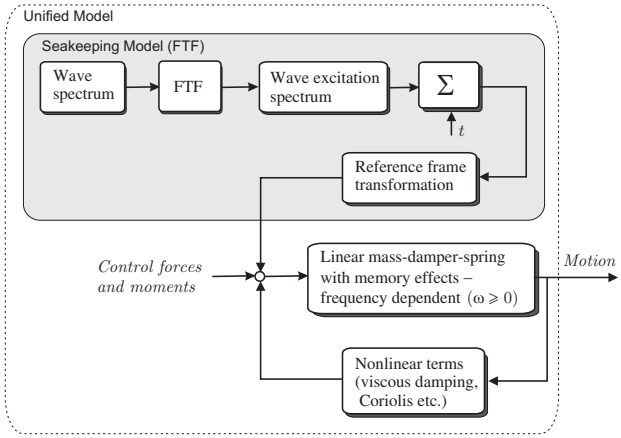

Figure 7: Unified time-domain model for maneuvering and control in a seaway [Perez and Fossen, 2004].

The main problem in doing this is that (22) depends on both the time and the frequency ω. In this model the wave loads are added as an external force and $\tau_{2,\text{FK+diff}}$ is computed from the FTF given by (32), see Figure 7.

For linear systems, the frequency-dependent coefficients $A_{22}(\omega)$ and $B_{22}(\omega)$ in (22) can be transformed to an equivalent time-domain representation thanks to the results of Cummins [1962] and Ogilvie [1964], see Appendix A:

$$[m + A_{22}(\infty)]\,\dot{v} + B_{22}(\infty)v + \int_0^t K_{22}(t-\tau)v(\tau)d\tau = \tau_{2,\text{env}} + \tau_2 \quad (35)$$

In (22) only the Froude-Krylov and diffraction excitation force $\tau_{2,\text{FK+diff}}$ (1st-order wave load) was considered. However, in the time-domain other environmental excitation forces like wave drift (2nd-order wave loads), wind and currents can be added directly such that:

$$\tau_{2,\text{env}} = \tau_{2,\text{FK+diff}} + \tau_{2,\text{drift}} + \tau_{2,\text{wind}} + \tau_{2,\text{currents}} \quad (36)$$

where $\tau_{2,\text{drift}}$ is the wave drift force, $\tau_{2,\text{wind}}$ is the wind force, and $\tau_{2,\text{currents}}$ is the current force. Within the framework of linear wave theory, the 1st-order motions are observed as zero mean oscillations, while 2nd-order terms represent the slowly-varying drift forces.

The integral term (impulse response) in (35) is referred to as the *memory effect* of the fluid and:

$$A_{22}(\infty) = \lim_{\omega\to\infty} A_{22}(\omega) = \textit{constant} \quad (37)$$

$$B_{22}(\infty) = \lim_{\omega\to\infty} B_{22}(\omega) = \textit{constant} \quad (38)$$

If the ship carries outs a harmonic oscillation $y(t) = \cos(\omega t)$, it can easily be shown by combining (22) and (35) that the impulse response function $K_{22}(t)$ in Figure 6 can be computed from one of the following equations [Ogilvie, 1964]:

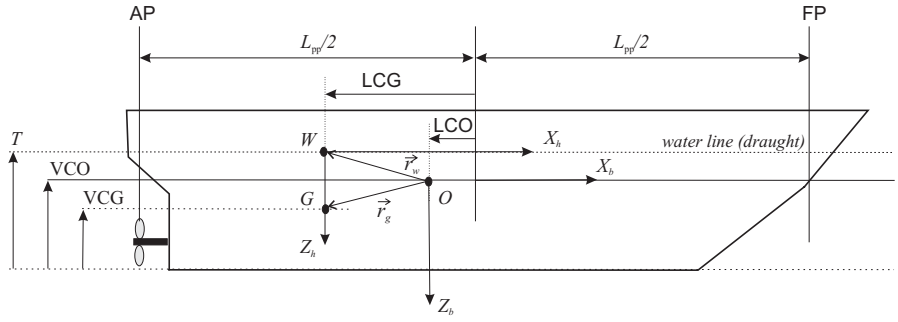

Figure 8: Definitions of coordinate origins: W (water line), G (centre of gravity), and O (equations of motion). The *h*-frame is located in W and the *b*-frame is located in O. The variables LCG, VCG, and T are defined by the hull while LCO and VCO are user inputs [Fossen and Smogeli, 2004].

$$
\begin{aligned}
K_{22}(t) &= \frac{2}{\pi}\int_0^\infty [B_{22}(\omega) - B_{22}(\infty)]\cos(\omega t)d\omega \\
K_{22}(t) &= -\frac{2}{\pi}\int_0^\infty \omega[A_{22}(\omega) - A_{22}(\infty)]\sin(\omega t)d\omega
\end{aligned}
$$

Thie model (35) has the advantage that it represents the wave-induced forces in the time-domain, giving a more physical description of the different sea states. Solving (35) for different environmental forces $\tau_{2,\mathrm{env}}$ gives responses y and v that include the frequency-dependent hydrodynamic motions. Maneuvering theory, on the contrary, is limited to calm water, i.e. $\omega = 0$.

The model (35) represents an important step towards a unified model for maneuvering and seakeeping. This is extended to 6 DOF in Section 5.

4 Kinematics

The kinematic transformations needed to represent the equations of motion in the different coordinate systems are presented in this section.

4.1 Coordinate Systems

Three orthogonal coordinate systems are used to describe the motions in 6 DOF [Fossen and Smogeli, 2004], see Figures 1 and 8:

- **North-East-Down frame (n-frame):** The *n*-frame $X_nY_nZ_n$ is assumed fixed on the Earth surface with the X_n-axis pointing North, the Y_n-axis pointing East, and the Z_n-axis down of the Earth tangent plane. The *n*-frame position $\mathbf{p}^n = [n, e, d]^\top$ and Euler angles $\mathbf{\Theta} = [\phi, \theta, \psi]^\top$ are defined in terms of the vector:

$$\boldsymbol{\eta} = [(\mathbf{p}^n)^\top, \mathbf{\Theta}^\top]^\top = [n, e, d, \phi, \theta, \psi]^\top \qquad (39)$$

- **Hydrodynamic frame (h-frame):** The hydrodynamic forces and moments are defined in a steadily translating *hydrodynamic coordinate system* $X_hY_hZ_h$ moving along the path of the ship with the constant speed $U \geq 0$ with respect to the *n*-frame. The X_hY_h-plane is parallel to the still water surface, and the ship carries out oscillations around the moving frame $X_hY_hZ_h$. The Z_h-axis is positive downwards, the Y_h-axis is positive towards starboard, and the X_h-axis is positive forwards. This is also referred to as the *equilibrium axis system* [Bailey *et al.*, 1998]. The coordinate origin of the *h*-frame is denoted *W*. The *n*-frame generalized position vector is:

$$
\begin{aligned}
\delta\boldsymbol{\eta}^* &= [\delta\eta_1^*, \delta\eta_2^*, \delta\eta_3^*, \delta\eta_4^*, \delta\eta_5^*, \delta\eta_6^*]^\top \\
&= [\delta n, \delta e, \delta d, \delta\phi, \delta\phi, \delta\psi]^\top \qquad (40)
\end{aligned}
$$

where δ denotes differential positions/angles with respect to the moving *n*-frame.

- **Body-fixed frame (b-frame):** The *b*-frame $X_bY_bZ_b$ is fixed to the hull, see Figure 1. The coordinate origin is denoted *O* and is located on the center line a distance *LCO* relative to $L_{pp}/2$ (positive backwards) and a distance *VCO* relative to the baseline (positive upwards). The center of gravity *G* with respect to *O* is located at $\mathbf{r}_g^b = [x_g, y_g, z_g]^\top$ while the *h*-frame origin *W* with respect to *O* is located at $\mathbf{r}_w^b = [x_w, y_w, z_w]^\top$. The X_b-axis is positive toward the bow and the X_h-axis is parallel to the mean X_b-axis, the Y_b-axis is positive towards starboard, and the Z_b-axis is positive downward. Consequently, the body-fixed *b*-frame

carries out oscillations $\delta\boldsymbol{\Theta} = [\delta\phi, \delta\theta, \delta\psi]^\top$ about the steadily translating *h*-frame. The *b*-frame linear velocities $\mathbf{v}_o^b = [u, v, w]^\top$ in *O* and angular velocities $\boldsymbol{\omega}_{bn}^b = [p, q, r]^\top$ with respect to the *n*-frame are denoted as:

$$\boldsymbol{\nu} = [(\mathbf{v}_o^b)^\top, (\boldsymbol{\omega}_{bn}^b)^\top]^\top = [u, v, w, p, q, r]^\top \quad (41)$$

The nominal generalized velocity vector is denoted as $\bar{\boldsymbol{\nu}} = [U, 0, 0, 0, 0, 0]^\top$. Hence:

$$\boldsymbol{\nu} = \bar{\boldsymbol{\nu}} + \delta\boldsymbol{\nu} \quad (42)$$

where $\delta\boldsymbol{\nu} = [\delta u, \delta v, \delta w, \delta p, \delta q, \delta r]^\top$ is a vector of differential velocities.

4.2 Generalized Velocity Transformation

It is convenient to define the vectors without reference to a coordinate frame (*coordinate free vector*). A vector $\vec{v}$ is defined by its magnitude and direction. The vector $\vec{v}_0$ in the point *O* decomposed in reference frame n is denoted as $\mathbf{v}_0^n$, which is also referred to as a *coordinate vector*.

The linear velocity $\vec{v}_w$ of *W* and the angular velocity $\vec{\omega}_{hn}$ of the h-frame with respect to the n-frame are:

$$\vec{v}_w = \vec{v}_o + \vec{\omega}_{bn} \times \vec{r}_w \quad (43)$$
$$\vec{\omega}_{hn} = \vec{\omega}_{bn} \quad (44)$$

where $\vec{\omega}_{bn}$ is the angular velocity of the b-frame with respect to the n-frame, and $\vec{r}_w$ is the vector from *O* to *W*. Decomposing these vectors into the *b*-frame gives:

$$\mathbf{v}_w^b = \mathbf{v}_o^b + \boldsymbol{\omega}_{bn}^b \times \mathbf{r}_w^b \quad (45)$$
$$\boldsymbol{\omega}_{hn}^b = \boldsymbol{\omega}_{bn}^b \quad (46)$$

The vector cross product $\times$ is defined in terms of the matrix $\mathbf{S}(\mathbf{r}_o^b) \in SS(3)$ (skew-symmetric matrix of order 3) such that:

$$\boldsymbol{\omega}_{bn}^b \times \mathbf{r}_w^b = -\mathbf{r}_w^b \times \boldsymbol{\omega}_{bn}^b = -\mathbf{S}(\mathbf{r}_w^b)\boldsymbol{\omega}_{bn}^b = \mathbf{S}(\mathbf{r}_w^b)^\top \boldsymbol{\omega}_{bn}^b \quad (47)$$

where:

$$\mathbf{S}(\mathbf{r}_w^b) = -\mathbf{S}^\top(\mathbf{r}_w^b) = \begin{bmatrix} 0 & -z_w & y_w \\ z_w & 0 & -x_w \\ -y_w & x_w & 0 \end{bmatrix} \quad (48)$$

Define the transformation matrix:

$$\mathbf{H}(\mathbf{r}_w^b) \triangleq \begin{bmatrix} \mathbf{I}_{3\times 3} & \mathbf{S}(\mathbf{r}_w^b)^\top \\ \mathbf{0}_{3\times 3} & \mathbf{I}_{3\times 3} \end{bmatrix} \quad (49)$$

Then it follows that:

$$\begin{bmatrix} \mathbf{v}_w^b \\ \boldsymbol{\omega}_{hn}^b \end{bmatrix} = \mathbf{H}(\mathbf{r}_w^b) \begin{bmatrix} \mathbf{v}_o^b \\ \boldsymbol{\omega}_{bn}^b \end{bmatrix} \quad (50)$$

4.3 Kinematics (b-frame to h-frame)

The transformation from the b-frame to the h-frame is done in terms of the small angle rotation matrices:

$$\mathbf{R}_b^h(\delta\boldsymbol{\Theta}) \triangleq \mathbf{R}_{z,\delta\psi}\mathbf{R}_{y,\delta\theta}\mathbf{R}_{x,\delta\phi} \quad (51)$$

where $\delta\psi$, $\delta\theta$, and $\delta\phi$ are oscillations of the *b*-frame with respect to the *h*-frame. These angles are related to ϕ, θ, and ψ according to:

$$\delta\phi = \phi \quad (52)$$
$$\delta\theta = \theta \quad (53)$$
$$\delta\psi = \psi - \frac{1}{T}\int_t^{t+T} \psi(\tau)d\tau \quad (54)$$

Hence, $\delta\psi$ can be understood as the oscillation about the average yaw angle in a given period T (s).

The principal rotations (small angle assumption) are:

$$\mathbf{R}_{x,\delta\phi} = \begin{bmatrix} 1 & 0 & 0 \\ 0 & 1 & -\delta\phi \\ 0 & \delta\phi & 1 \end{bmatrix} \quad (55)$$

$$\mathbf{R}_{y,\delta\theta} = \begin{bmatrix} 1 & 0 & \delta\theta \\ 0 & 1 & 0 \\ -\delta\theta & 0 & 1 \end{bmatrix} \quad (56)$$

$$\mathbf{R}_{z,\delta\psi} = \begin{bmatrix} 1 & -\delta\psi & 0 \\ \delta\psi & 1 & 0 \\ 0 & 0 & 1 \end{bmatrix} \quad (57)$$

Thus $\mathbf{R}_b^h(\delta\boldsymbol{\Theta}) \in SO(3)$ becomes:

$$\mathbf{R}_b^h(\delta\boldsymbol{\Theta}) = \begin{bmatrix} 1 & -\delta\psi & \delta\theta \\ \delta\psi & 1 & -\delta\phi \\ -\delta\theta & \delta\phi & 1 \end{bmatrix} \quad (58)$$

From (50) it follows that:

$$\begin{bmatrix} \mathbf{R}_h^b(\delta\boldsymbol{\Theta}) & \mathbf{0}_{3\times 3} \\ \mathbf{0}_{3\times 3} & \mathbf{R}_h^b(\delta\boldsymbol{\Theta}) \end{bmatrix} \begin{bmatrix} \mathbf{v}_w^h \\ \boldsymbol{\omega}_{hn}^h \end{bmatrix} = \mathbf{H}(\mathbf{r}_w^b) \begin{bmatrix} \mathbf{v}_o^b \\ \boldsymbol{\omega}_{bn}^b \end{bmatrix}$$

where $\mathbf{R}_h^b(\delta\boldsymbol{\Theta}) = \mathbf{R}_b^h(\delta\boldsymbol{\Theta})^{-1}$. Consequently, the velocity transformation between the *h* and *b* frames becomes:

$$\mathbf{v}_w^h = \mathbf{R}_b^h(\delta\boldsymbol{\Theta})\left[\mathbf{v}_o^b + \mathbf{S}(\mathbf{r}_w^b)^\top \boldsymbol{\omega}_{bn}^b\right] \quad (59)$$
$$\boldsymbol{\omega}_{hn}^h = \mathbf{R}_b^h(\delta\boldsymbol{\Theta})\boldsymbol{\omega}_{bn}^b \quad (60)$$

Since the *h-frame* moves along the path of the ship with the constant speed U, (59)–(60) can be expanded as:

$$\begin{bmatrix} \delta\dot{\eta}_1^* + U \\ \delta\dot{\eta}_2^* \\ \delta\dot{\eta}_3^* \end{bmatrix} = \mathbf{R}_b^h(\delta\boldsymbol{\Theta}) \begin{bmatrix} u \\ v \\ w \end{bmatrix} + \mathbf{R}_b^h(\delta\boldsymbol{\Theta})\mathbf{S}(\mathbf{r}_w^b)^\top \begin{bmatrix} p \\ q \\ r \end{bmatrix} \quad (61)$$

$$\begin{bmatrix} \delta\dot{\eta}_4^* \\ \delta\dot{\eta}_5^* \\ \delta\dot{\eta}_6^* \end{bmatrix} = \mathbf{R}_b^h(\delta\boldsymbol{\Theta}) \begin{bmatrix} p \\ q \\ r \end{bmatrix} \quad (62)$$

Note that the total *b-frame* velocity in the horizontal plane is $u = U + \delta u$ and $\delta v = v$ since $\delta\psi$ is small, whereas $\delta w = w, \delta p = p, \delta q = q$, and $\delta r = r$.

In the forthcoming we will consider slender ships with starboard/port symmetry implying that DOF 1,3,5 can be decoupled from DOF 2,4,6. Decoupling between the *longitudinal* and *lateral* modes, $y_g = y_w = 0$, and neglecting higher-order δ-terms in (61)–(62), i.e. linear theory, gives:

$$\begin{aligned}
\delta\dot{\eta}_1^* &= u - U + z_w q = \delta u + z_w \delta q && (63)\\
\delta\dot{\eta}_2^* &= (U + \delta u)\delta\psi + \delta v + x_w \delta r - z_w \delta p \\
&\approx \delta v + x_w \delta r - z_w \delta p + U\delta\psi && (64)\\
\delta\dot{\eta}_3^* &= -(U + \delta u)\delta\theta + \delta w - x_w \delta q \\
&\approx \delta w - x_w \delta q - U\delta\theta && (65)\\
\delta\dot{\eta}_4^* &= \delta p && (66)\\
\delta\dot{\eta}_5^* &= \delta q && (67)\\
\delta\dot{\eta}_6^* &= \delta r && (68)
\end{aligned}$$

Time differentiation of (63)–(68) gives:

$$\begin{aligned}
\delta\ddot{\eta}_1^* &= \delta\dot{u} + z_w \delta\dot{q} && (69)\\
\delta\ddot{\eta}_2^* &= \delta\dot{v} + x_w \delta\dot{r} - z_w \delta\dot{p} + U\delta r && (70)\\
\delta\ddot{\eta}_3^* &= \delta\dot{w} - x_w \delta\dot{q} - U\delta q && (71)\\
\delta\ddot{\eta}_4^* &= \delta\dot{p} && (72)\\
\delta\ddot{\eta}_5^* &= \delta\dot{q} && (73)\\
\delta\ddot{\eta}_6^* &= \delta\dot{r} && (74)
\end{aligned}$$

Let ω_e denote the frequency of encounter:

$$\omega_e = \omega - \frac{U}{g}\omega^2 \cos\psi_r \qquad (75)$$

where U is the forward speed, g is the acceleration of gravity, and ψ_r is the relative angle of the incident waves. Under the assumption of *sinusoidal motions* in pitch and yaw, with frequency ω_e and amplitudes A_1 and A_2, it follows that:

$$\begin{array}{ll}
\delta\theta = A_1 \sin\omega_e t & \delta\psi = A_2 \sin\omega_e t \\
\delta q = A_1\omega_e \cos\omega_e t & \delta r = A_2\omega_e \cos\omega_e t \\
\delta\dot{q} = -A_1\omega_e^2 \sin\omega_e t & \delta\dot{r} = -A_2\omega_e^2 \sin\omega_e t
\end{array} \qquad (76)$$

This implies that:

$$\delta\psi = -\frac{1}{\omega_e^2}\delta\dot{r}, \quad \delta\theta = -\frac{1}{\omega_e^2}\delta\dot{q} \qquad (77)$$

such that the velocity transformations (63)–(68) can be written:

$$\begin{aligned}
\delta\dot{\eta}_1^* &= \delta u + z_w \delta q && (78)\\
\delta\dot{\eta}_2^* &= \delta v + x_w \delta r - z_w \delta p - \frac{U}{\omega_e^2}\delta\dot{r} && (79)\\
\delta\dot{\eta}_3^* &= \delta w - x_w \delta q + \frac{U}{\omega_e^2}\delta\dot{q} && (80)\\
\delta\dot{\eta}_4^* &= \delta p && (81)\\
\delta\dot{\eta}_5^* &= \delta q && (82)\\
\delta\dot{\eta}_6^* &= \delta r && (83)
\end{aligned}$$

The velocity (78)–(83) and acceleration (69)–(74) transformations can now be written in compact forms by defining two transformation matrices $\mathbf{J}^* \in \mathbb{R}^{6\times 6}$ and $\mathbf{L}^* \in \mathbb{R}^{6\times 6}$ according to:

$$\begin{aligned}
\delta\dot{\boldsymbol{\eta}}^* &= \mathbf{J}^*\delta\boldsymbol{\nu} - \frac{U}{\omega_e^2}\mathbf{L}^*\delta\dot{\boldsymbol{\nu}} && (84)\\
\delta\ddot{\boldsymbol{\eta}}^* &= \mathbf{J}^*\delta\dot{\boldsymbol{\nu}} + U\mathbf{L}^*\delta\boldsymbol{\nu} && (85)
\end{aligned}$$

where $\delta\boldsymbol{\nu} = [\delta u, \delta v, \delta w, \delta p, \delta q, \delta r]^\top$ and:

$$\mathbf{J}^* \triangleq \mathbf{H}(\mathbf{r}_w^b) = \begin{bmatrix}
1 & 0 & 0 & 0 & z_w & 0 \\
0 & 1 & 0 & -z_w & 0 & x_w \\
0 & 0 & 1 & 0 & -x_w & 0 \\
0 & 0 & 0 & 1 & 0 & 0 \\
0 & 0 & 0 & 0 & 1 & 0 \\
0 & 0 & 0 & 0 & 0 & 1
\end{bmatrix} \qquad (86)$$

$$\mathbf{L}^* \triangleq \begin{bmatrix}
0 & 0 & 0 & 0 & 0 & 0 \\
0 & 0 & 0 & 0 & 0 & 1 \\
0 & 0 & 0 & 0 & -1 & 0 \\
0 & 0 & 0 & 0 & 0 & 0 \\
0 & 0 & 0 & 0 & 0 & 0 \\
0 & 0 & 0 & 0 & 0 & 0
\end{bmatrix} \qquad (87)$$

For station-keeping and low-speed maneuvering, i.e. $U = 0$, we have that $\dot{\boldsymbol{\eta}}^* = \delta\dot{\boldsymbol{\eta}}^*$ and $\boldsymbol{\nu} = \delta\boldsymbol{\nu}$. This gives a speed independent transformation [Fossen and Smogeli, 2004]:

$$\begin{aligned}
\dot{\boldsymbol{\eta}}^* &= \mathbf{J}^*\boldsymbol{\nu} && (88)\\
\ddot{\boldsymbol{\eta}}^* &= \mathbf{J}^*\dot{\boldsymbol{\nu}} && (89)
\end{aligned}$$

4.4 Kinematics (b-frame to n-frame)

The velocity transformation between the *b* and *n* frames is:

$$\mathbf{v}_o^n = \mathbf{R}_b^n(\boldsymbol{\Theta})\mathbf{v}_o^b \qquad (90)$$

where the Euler angle rotation matrix (zyx-convention) between the n and b frames is defined as the product of the three principal rotations:

$$\mathbf{R}_b^n(\boldsymbol{\Theta}) \triangleq \mathbf{R}_{z,\psi}\mathbf{R}_{y,\theta}\mathbf{R}_{x,\phi} \qquad (91)$$

Thus $\mathbf{R}_b^n(\boldsymbol{\Theta}) \in SO(3)$ becomes:

$$\mathbf{R}_b^n(\boldsymbol{\Theta}) = \begin{bmatrix} \mathrm{c}\psi\mathrm{c}\theta & -\mathrm{s}\psi\mathrm{c}\phi + \mathrm{c}\psi\mathrm{s}\theta\mathrm{s}\phi & \mathrm{s}\psi\mathrm{s}\phi + \mathrm{c}\psi\mathrm{c}\phi\mathrm{s}\theta \\ \mathrm{s}\psi\mathrm{c}\theta & \mathrm{c}\psi\mathrm{c}\phi + \mathrm{s}\phi\mathrm{s}\theta\mathrm{s}\psi & -\mathrm{c}\psi\mathrm{s}\phi + \mathrm{s}\theta\mathrm{s}\psi\mathrm{c}\phi \\ -\mathrm{s}\theta & \mathrm{c}\theta\mathrm{s}\phi & \mathrm{c}\theta\mathrm{c}\phi \end{bmatrix} \tag{92}$$

The Euler rates satisfy:

$$\dot{\boldsymbol{\Theta}} = \mathbf{T}_\Theta(\boldsymbol{\Theta})\boldsymbol{\omega}_{bn}^b \tag{93}$$

where $\mathbf{T}_\Theta(\boldsymbol{\Theta}) \in \mathbb{R}^{3\times3}$ is the Euler angle attitude transformation matrix:

$$\mathbf{T}_\Theta(\boldsymbol{\Theta}) = \begin{bmatrix} 1 & \mathrm{s}\phi\mathrm{t}\theta & \mathrm{c}\phi\mathrm{t}\theta \\ 0 & \mathrm{c}\phi & -\mathrm{s}\phi \\ 0 & \mathrm{s}\phi/\mathrm{c}\theta & \mathrm{c}\phi/\mathrm{c}\theta \end{bmatrix}, \qquad \theta \neq \pm 90^o \tag{94}$$

Consequently:

$$\dot{\boldsymbol{\eta}} = \mathbf{J}(\boldsymbol{\Theta})\boldsymbol{\nu} \tag{95}$$

where $\mathbf{J}(\boldsymbol{\Theta}) \in \mathbb{R}^{6\times6}$ is the velocity transformation matrix:

$$\mathbf{J}(\boldsymbol{\Theta}) = \begin{bmatrix} \mathbf{R}_b^n(\boldsymbol{\Theta}) & \mathbf{0}_{3\times3} \\ \mathbf{0}_{3\times3} & \mathbf{T}_\Theta(\boldsymbol{\Theta}) \end{bmatrix}, \qquad \theta \neq \pm 90^o \tag{96}$$

5 Unified Model for Ship Maneuvering and Control in a Seaway

A unified model for maneuvering and seakeeping is attractive for real-time simulation and control design. The presented model is motivated by the results of Bishop and Price [1981] and Bailey *et al.* [1998]. The 6 DOF ship equations of motion in a seaway should also give new insight into the computational efforts required to implement the equations in a real-time simulator for training purposes and model-based ship control systems.

5.1 Frequency Domain Equation

Seakeeping Theory (h-frame formulation)

The 6 DOF seakeeping model is usually formulated in the *h-frame* using Newton's 2nd law:

$$\mathbf{M}_{RB}^*\delta\ddot{\boldsymbol{\eta}}^* = \delta\boldsymbol{\tau}_H^* + \delta\boldsymbol{\tau}_{\mathrm{FK+diff}}^* + \delta\boldsymbol{\tau}^* \tag{97}$$

where $\delta\boldsymbol{\tau}_{\mathrm{FK+diff}}^*$ is a vector of generalized *Froude-Krylov* and *diffraction* forces and $\delta\boldsymbol{\tau}^*$ is the differential generalized control forces satisfying $\boldsymbol{\tau}^* = \delta\bar{\boldsymbol{\tau}}^* + \delta\boldsymbol{\tau}^*$ where $\delta\bar{\boldsymbol{\tau}}^*$ is the steady-state control input needed to obtain $u = U$. The generalized hydrodynamic added mass, damping, and restoring forces are [Faltinsen, 1990]:

$$\delta\boldsymbol{\tau}_H = -\mathbf{A}^*(\omega_e)\delta\ddot{\boldsymbol{\eta}}^* - \mathbf{B}^*(\omega_e)\delta\dot{\boldsymbol{\eta}}^* - \mathbf{g}^*(\delta\boldsymbol{\eta}^*) \tag{98}$$

The frequency-dependent hydrodynamic matrices $\mathbf{A}^*(\omega_e)$ and $\mathbf{B}^*(\omega_e)$ are usually computed using a potential theory program, see Section 7.1. The resulting model is referred to as the *frequency domain equation*:

$$\begin{aligned}[\mathbf{M}_{RB}^* + \mathbf{A}^*(\omega_e)]\,\delta\ddot{\boldsymbol{\eta}}^* + \mathbf{B}^*(\omega_e)\delta\dot{\boldsymbol{\eta}}^* \\ +\mathbf{C}^*\delta\boldsymbol{\eta}^* = \delta\boldsymbol{\tau}_{\mathrm{FK+diff}}^* + \delta\boldsymbol{\tau}^*\end{aligned} \tag{99}$$

where we have assumed that the restoring forces are linear:

$$\mathbf{g}^*(\delta\boldsymbol{\eta}^*) = \mathbf{C}^*\delta\boldsymbol{\eta}^* \tag{100}$$

This is a good assumption for floating vessels at zero and moderate speeds [Faltinsen, 1990].

Seakeeping Theory (b-frame formulation)

In order to derive the *b-frame* seakeeping equations we will make use of the transformations derived in Section 4.3. Recall that the velocity and acceleration in the *b-frame* can be transformed to the *h-frame* by:

$$\delta\dot{\boldsymbol{\eta}}^* = \mathbf{J}^*\delta\boldsymbol{\nu} - \frac{U}{\omega_e^2}\mathbf{L}^*\delta\dot{\boldsymbol{\nu}} \tag{101}$$

$$\delta\ddot{\boldsymbol{\eta}}^* = \mathbf{J}^*\delta\dot{\boldsymbol{\nu}} + U\mathbf{L}^*\delta\boldsymbol{\nu} \tag{102}$$

Substituting these expressions into (99) and premultiplication with $\mathbf{J}^{*\top}$ gives:

$$\begin{aligned}\mathbf{J}^{*\top}(\mathbf{M}_{RB}^* + \mathbf{A}^*(\omega_e))\,[\mathbf{J}^*\delta\dot{\boldsymbol{\nu}} + U\mathbf{L}^*\delta\boldsymbol{\nu}] \\ + \mathbf{J}^{*\top}\mathbf{B}^*(\omega_e)\left[\mathbf{J}^*\delta\boldsymbol{\nu} - \frac{U}{\omega_e^2}\mathbf{L}^*\delta\dot{\boldsymbol{\nu}}\right] \\ + \mathbf{J}^{*\top}\mathbf{g}^*(\delta\boldsymbol{\eta}^*) = \mathbf{J}^{*\top}(\delta\boldsymbol{\tau}_{\mathrm{FK+diff}}^* + \delta\boldsymbol{\tau}^*)\end{aligned}$$

The generalized inertia matrix $\mathbf{M}_{RB}$ can be transformed between the *b-frame* and the *h-frame* using (assuming small oscillations):

$$\mathbf{M}_{RB} = \mathbf{J}^{*\top}\mathbf{M}_{RB}^*\mathbf{J}^* \tag{103}$$

Then:

$$\begin{aligned}\left[\mathbf{M}_{RB} + \tilde{\mathbf{M}}_A(\omega_e)\right]\delta\dot{\boldsymbol{\nu}} + \left[\mathbf{C}_{RB} + \tilde{\mathbf{C}}_A(\omega_e)\right]\delta\boldsymbol{\nu} \\ + \tilde{\mathbf{D}}(\omega_e)\delta\boldsymbol{\nu} + \mathbf{g}(\delta\boldsymbol{\eta}) = \delta\boldsymbol{\tau}_{\mathrm{FK+diff}} + \delta\boldsymbol{\tau}\end{aligned} \tag{104}$$

where:

$$\begin{aligned}\tilde{\mathbf{M}}_A(\omega_e) &= \mathbf{J}^{*\top}\mathbf{A}^*(\omega_e)\mathbf{J}^* - \frac{U}{\omega_e^2}\mathbf{J}^{*\top}\mathbf{B}^*(\omega_e)\mathbf{L}^* \\ \tilde{\mathbf{D}}(\omega_e) &= \mathbf{J}^{*\top}\mathbf{B}^*(\omega_e)\mathbf{J}^* \\ \mathbf{C}_{RB} &= U\mathbf{J}^{*\top}\mathbf{M}_{RB}^*\mathbf{L}^* \\ \tilde{\mathbf{C}}_A(\omega_e) &= U\mathbf{J}^{*\top}\mathbf{A}^*(\omega_e)\mathbf{L}^* \\ \mathbf{g}(\delta\boldsymbol{\eta}) &= \mathbf{J}^{*\top}\mathbf{g}^*(\delta\boldsymbol{\eta}^*) \overset{\text{linear}}{\Rightarrow} (\mathbf{G} = \mathbf{J}^{*\top}\mathbf{C}^*\mathbf{J}^*) \\ \delta\boldsymbol{\tau}_{\mathrm{FK+diff}} &= \mathbf{J}^{*\top}\delta\boldsymbol{\tau}_{\mathrm{FK+diff}}^* \\ \delta\boldsymbol{\tau} &= \mathbf{J}^{*\top}\delta\boldsymbol{\tau}^*\end{aligned}$$

Notice that this transformation generates two new matrices $\mathbf{C}_{RB}$ and $\tilde{\mathbf{C}}_A(\omega_e)$ which are recognized as the *Coriolis and centripetal matrices* due to rigid-body and frequency-dependent added mass, respectively [Fossen, 2002].

For $\mathbf{r}_w^b = [0, 0, z_w]^\top$ we get:

$$\tilde{\mathbf{C}}_{RB}{=}U \begin{bmatrix} & 0 & 0 \\ & 0 & m \\ \mathbf{0}_{6\times 4} & -m & 0 \\ & 0 & -mz_w \\ & 0 & 0 \\ & 0 & 0 \end{bmatrix}$$

$$\tilde{\mathbf{C}}_A{=}U \begin{bmatrix} & -A_{13} & 0 \\ & 0 & A_{22} \\ \mathbf{0}_{6\times 4} & -A_{33} & 0 \\ & 0 & (A_{42} - A_{22}z_w) \\ & -(A_{53} + A_{13}z_w) & 0 \\ & 0 & A_{62} \end{bmatrix}$$

For notational convenience we will rewrite (104) as:

$$\left[\mathbf{M}_{RB} + \tilde{\mathbf{M}}_A(\omega_e)\right] \delta\dot{\boldsymbol{\nu}} + \mathbf{C}_{RB}\delta\boldsymbol{\nu} + \tilde{\mathbf{N}}(\omega_e)\delta\boldsymbol{\nu}{+}\mathbf{g}(\delta\boldsymbol{\eta}){=}\delta\boldsymbol{\tau}_{\text{FK+diff}}{+}\delta\boldsymbol{\tau} \quad (105)$$

where $\tilde{\mathbf{N}}(\omega)$ contains the linear frequency-dependent Coriolis, centripetal, and damping terms:

$$\tilde{\mathbf{N}}(\omega_e){=}\,\tilde{\mathbf{C}}_A(\omega_e){+}\tilde{\mathbf{D}}(\omega_e) \quad (106)$$

Thanks to the special structure of $\mathbf{L}^*$, we have:

$$\mathbf{L}^* = \mathbf{L}^*\mathbf{J}^* \quad (107)$$

such that:

$$\tilde{\mathbf{M}}_A(\omega_e) = \mathbf{J}^{*\top}\left[\mathbf{A}^*(\omega_e){-}\frac{U}{\omega_e^2}\mathbf{B}^*(\omega_e)\mathbf{L}^*\right]\mathbf{J}^* \quad (108)$$

$$\tilde{\mathbf{N}}(\omega_e) = \mathbf{J}^{*\top}\left[\mathbf{B}^*(\omega_e) + U\mathbf{A}^*(\omega_e)\mathbf{L}^*\right]\mathbf{J}^* \quad (109)$$

5.2 Time-Domain Solution

Since (108)–(109) are linear transformations corresponding to transfer functions, the frequency-dependent equation (105) can be transformed to the time-domain using impulse response functions or state-space models [Kristiansen and Egeland, 2003] [Kristiansen, 2005].

The time-domain solution for (105) is (Appendix A):

$$\left[\mathbf{M}_{RB} + \tilde{\mathbf{M}}_A(\infty)\right]\delta\dot{\boldsymbol{\nu}}{+}\mathbf{C}_{RB}\delta\boldsymbol{\nu} + \tilde{\mathbf{N}}(\infty)\delta\boldsymbol{\nu} + \int_{-\infty}^{t}\mathbf{K}(t-\tau)\delta\boldsymbol{\nu}(\tau)d\tau{+}\mathbf{g}(\delta\boldsymbol{\eta}) {=}\delta\boldsymbol{\tau}_{\text{FK+diff}}{+}\delta\boldsymbol{\tau} \quad (110)$$

where $\mathbf{K}(t)$ is a matrix of impulse response functions:

$$\mathbf{K}(t) = \frac{2}{\pi}\int_0^\infty [\tilde{\mathbf{N}}(\omega_e) - \tilde{\mathbf{N}}(\infty)]\cos(\omega_e t)d\omega_e \quad (111)$$

and:

$$\tilde{\mathbf{M}}_A(\infty) = \mathbf{J}^{*\top}\mathbf{A}^*(\infty)\mathbf{J}^* \quad (112)$$

$$\tilde{\mathbf{N}}(\infty) = \mathbf{J}^{*\top}\left[\mathbf{B}^*(\infty) + U\mathbf{A}^*(\infty)\mathbf{L}^*\right]\mathbf{J}^* \quad (113)$$

For notational simplicity, we define:

$$\mathbf{M} \triangleq \mathbf{M}_{RB} + \tilde{\mathbf{M}}_A(\infty) \quad (114)$$

$$\mathbf{D} \triangleq \tilde{\mathbf{N}}(\infty) \quad (115)$$

$$\boldsymbol{\mu} \triangleq \int_{-\infty}^{t}\mathbf{K}(t-\tau)\delta\boldsymbol{\nu}(\tau)d\tau \quad (116)$$

where $\mathbf{M}$ is the generalized inertia matrix and $\mathbf{D}$ is the linear damping matrix. Hence (110) takes the form:

$$\mathbf{M}\delta\dot{\boldsymbol{\nu}}{+}\mathbf{C}_{RB}\delta\boldsymbol{\nu} + \mathbf{D}\delta\boldsymbol{\nu} + \boldsymbol{\mu}{+}\mathbf{g}(\delta\boldsymbol{\eta}) {=}\delta\boldsymbol{\tau}_{\text{FK+diff}}{+}\delta\boldsymbol{\tau} \quad (117)$$

Substituting the perturbation terms:

$$\delta\boldsymbol{\nu}{=}\boldsymbol{\nu} - \bar{\boldsymbol{\nu}} \quad (118)$$

$$\delta\boldsymbol{\tau}{=}\boldsymbol{\tau} - \bar{\boldsymbol{\tau}} \quad (119)$$

$$\delta\boldsymbol{\Theta}{=}\,\boldsymbol{\Theta} - \mathbf{0} = \boldsymbol{\Theta} \quad (120)$$

$$\delta\boldsymbol{\tau}_{\text{FK+diff}} = \boldsymbol{\tau}_{\text{FK+diff}} - \mathbf{0} = \boldsymbol{\tau}_{\text{FK+diff}} \quad (121)$$

into (117) gives:

$$\mathbf{M}\dot{\boldsymbol{\nu}}{+}\mathbf{C}_{RB}\boldsymbol{\nu} + \mathbf{D}\boldsymbol{\nu} + \boldsymbol{\mu}{+}\mathbf{g}(\boldsymbol{\eta}) = \boldsymbol{\tau}_{\text{FK+diff}}{+}\boldsymbol{\tau} + (\mathbf{C}_{RB}\bar{\boldsymbol{\nu}} + \mathbf{D}\bar{\boldsymbol{\nu}} - \bar{\boldsymbol{\tau}}) \quad (122)$$

The constant control input $\bar{\boldsymbol{\tau}} = \mathbf{C}_{RB}\bar{\boldsymbol{\nu}} + \mathbf{D}\bar{\boldsymbol{\nu}}$ corresponding to steady-state ($\delta\dot{\boldsymbol{\nu}} {=}\delta\boldsymbol{\nu} = \mathbf{0}$ and $\boldsymbol{\tau}_{\text{FK+diff}} = \mathbf{0}$) finally gives:

$$\dot{\boldsymbol{\eta}} = \mathbf{J}(\boldsymbol{\Theta})\boldsymbol{\nu} \quad (123)$$

$$\mathbf{M}\dot{\boldsymbol{\nu}}{+}\mathbf{C}_{RB}\boldsymbol{\nu} + \mathbf{D}\boldsymbol{\nu} + \boldsymbol{\mu}{+}\mathbf{g}(\boldsymbol{\eta}) = \boldsymbol{\tau}_{\text{FK+diff}}{+}\boldsymbol{\tau} \quad (124)$$

5.3 Adding Nonlinear Damping and Environmental Forces in the Time-Domain

The time-domain model (124) can be further extended to include nonlinear damping terms:

$$\boldsymbol{\tau}_n = -\mathbf{d}_n(\boldsymbol{\Theta}, \boldsymbol{\nu}) \quad (125)$$

and environmental forces due to wave drift, wind, and currents by writing:

$$\mathbf{M}\dot{\boldsymbol{\nu}}{+}\mathbf{C}_{RB}\boldsymbol{\nu} + \mathbf{D}\boldsymbol{\nu} + \boldsymbol{\mu}{+}\mathbf{d}_n(\boldsymbol{\Theta},\boldsymbol{\nu}){+}\mathbf{g}(\boldsymbol{\eta}) = \boldsymbol{\tau}_{\text{env}} + \boldsymbol{\tau} \quad (126)$$

where

$$\boldsymbol{\tau}_{\text{env}} = \underbrace{\boldsymbol{\tau}_{\text{FK+diff}} + \boldsymbol{\tau}_{\text{drift}}}_{\boldsymbol{\tau}_{\text{waves}}} + \boldsymbol{\tau}_{\text{wind}} + \boldsymbol{\tau}_{\text{currents}} \tag{127}$$

The equilibrium $\delta\dot{\boldsymbol{\nu}} = \delta\boldsymbol{\nu} = \mathbf{0}$ and $\boldsymbol{\tau}_{\text{env}} = \mathbf{0}$, corresponding to $u = U$ and $v = w = p = q = r = 0$, is obtained for the control input $\bar{\boldsymbol{\tau}} = \mathbf{C}_{RB}\bar{\boldsymbol{\nu}} + \mathbf{D}\bar{\boldsymbol{\nu}} + \mathbf{d}_n(\mathbf{0},\bar{\boldsymbol{\nu}})$.

5.3.1 Nonlinear Damping Terms

The nonlinear damping term $\boldsymbol{\tau}_n$ can be found from PMM experiments [Lewis, 1989].

The nonlinear parametrizations used in maneuvering theory are usually classified according to [Clarke, 2003]:

Truncated Taylor series expansions [Abkowitz, 1964]. For starboard/port symmetric vessels a vector of 3rd-order terms $\boldsymbol{\tau}_n = [\tau_{n1}, \tau_{n2}, ..., \tau_{n6}]^\top$ should be included in addition to linear damping, i.e.:

$$\begin{aligned}
\tau_{n1} &= X_{uuu}u^3 + X_{www}w^3 + X_{qqq}q^3 \\
&\quad + X_{uww}uw^2 + X_{uqq}uq^2 + \cdots \\
\tau_{n2} &= Y_{vvv}v^3 + Y_{ppp}p^3 + Y_{rrr}r^3 \\
&\quad + Y_{vpp}vp^2 + Y_{vrr}vr^2 + \cdots \\
&\quad \vdots \\
\tau_{n6} &= N_{rrr}r^3 + \cdots
\end{aligned}$$

Second-order modulus models have been proposed by Fedyaevsky and Sobolev [1963], Norrbin [1970], and Blanke and Christensen [1993] for instance. For the lateral motions $\boldsymbol{\tau}_n = [\tau_{n2}, \tau_{n4}, \tau_{n6}]^\top$, Blanke and Christensen [1993] give the following second-order modulus model:

$$\begin{aligned}
\tau_{n2} &= Y_{|u|v}\,|u|\,v + Y_{ur}ur + Y_{v|v|}v\,|v| + Y_{v|r|}v\,|r| \\
&\quad + Y_{r|v|}r\,|v| + Y_{\phi|uv|}\phi\,|uv| + Y_{\phi|ur|}\phi\,|ur| \\
&\quad + Y_{\phi uu}\phi u^2
\end{aligned}$$

$$\begin{aligned}
\tau_{n4} &= K_{|u|v}\,|u|\,v + K_{ur}ur + K_{v|v|}v\,|v| + K_{v|r|}v\,|r| \\
&\quad + K_{r|v|}r\,|v| + K_{\phi|uv|}\phi\,|uv| + K_{\phi|ur|}\phi\,|ur| \\
&\quad + K_{\phi uu}\phi\,u^2 + K_{|u|p}\,|u|\,p \\
&\quad + K_{p|p|}p\,|p| + K_{\phi\phi\phi}\phi^3
\end{aligned}$$

$$\begin{aligned}
\tau_{n6} &= N_{|u|v}\,|u|\,v + N_{|u|r}\,|u|\,r + N_{r|r|}r\,|r| + N_{r|v|}r\,|v| \\
&\quad + N_{\phi|uv|}\phi\,|uv| + N_{\phi u|r|}\phi u\,|r| \\
&\quad + N_{|p|p}|p|p + N_{|u|p}|u|p + N_{\phi u|u|}\phi u\,|u|
\end{aligned}$$

Several other models are available in the literature; see Fossen [1994, 2002], Bertram [2004], and Perez [2005] and references therein.

6 State-Space representation for the Unified Model

This section presents state-space models for effective simulation of the unified model in Section 5. The cases for forward and zero speed are treated separately.

6.1 Forward Speed State-Space Representation

Consider the unified model (126):

$$\mathbf{M}\dot{\boldsymbol{\nu}} + \mathbf{C}_{RB}\boldsymbol{\nu} + \mathbf{D}\boldsymbol{\nu} + \boldsymbol{\mu} + \mathbf{d}_n(\boldsymbol{\Theta},\boldsymbol{\nu}) + \mathbf{g}(\boldsymbol{\eta}) = \boldsymbol{\tau}_{\text{env}} + \boldsymbol{\tau} \tag{128}$$

where:

$$\boldsymbol{\mu} = \int_{-\infty}^{t} \mathbf{K}(t-\tau)\delta\boldsymbol{\nu}(\tau)d\tau \tag{129}$$

$$\mathbf{K}(t) = \frac{2}{\pi}\int_0^\infty [\tilde{\mathbf{N}}(\omega_e) - \tilde{\mathbf{N}}(\infty)]\cos(\omega_e t)d\omega_e \tag{130}$$

For causal systems:

$$\mathbf{K}(t) = \mathbf{0} \text{ for } t < 0 \tag{131}$$

such that:

$$\boldsymbol{\mu}(t) = \int_{-\infty}^{t} \mathbf{K}(t-\tau)\delta\boldsymbol{\nu}(\tau)d\tau \overset{\text{causal}}{=} \int_0^t \mathbf{K}(t-\tau)\delta\boldsymbol{\nu}(\tau)d\tau \tag{132}$$

where $\mathbf{K}(t-\tau)$ is the *retardation function.*

Kristiansen and Egeland [2003] and Kristiansen [2005] have developed a state-space formulation for $\boldsymbol{\mu}$. If $\delta\boldsymbol{\nu}$ is a unit impulse, then $\boldsymbol{\mu}$ given by (132) will be an *impulse response* function. Consequently, $\boldsymbol{\mu}$ can be approximated by a linear reduced-order state-space model:

$$\dot{\boldsymbol{\chi}} = \mathbf{A}_r\boldsymbol{\chi} + \mathbf{B}_r\delta\boldsymbol{\nu}, \qquad \boldsymbol{\chi}(0) = \mathbf{0} \tag{133}$$

$$\boldsymbol{\mu} = \mathbf{C}_r\boldsymbol{\chi} + \mathbf{D}_r\delta\boldsymbol{\nu} \tag{134}$$

where $(\mathbf{A}_r, \mathbf{B}_r, \mathbf{C}_r, \mathbf{D}_r)$ are constant matrices of appropriate dimensions and $\delta\boldsymbol{\nu} = \boldsymbol{\nu} - \bar{\boldsymbol{\nu}}$. Applying the *Laplace transformation* to (133)–(134), the *damping* term (132) can be written as:

$$\boldsymbol{\mu}(s) = \mathbf{D}_{\text{mem}}(s)\delta\boldsymbol{\nu}(s) \tag{135}$$

where $\mathbf{D}_{\text{mem}}(s) \in \mathbb{R}^{6\times 6}$ is a transfer function matrix. Notice that the filter:

$$\mathbf{D}_{\text{mem}}(s) = \mathbf{C}_r(s\mathbf{I} - \mathbf{A}_r)^{-1}\mathbf{B}_r + \mathbf{D}_r \tag{136}$$

now contains the *memory effect* of the fluid. The resulting nonlinear state-space model is:

$$\dot{\boldsymbol{\eta}} = \mathbf{J}(\boldsymbol{\Theta})\boldsymbol{\nu} \tag{137}$$

$$\mathbf{M}\dot{\boldsymbol{\nu}} + \mathbf{C}_{RB}\boldsymbol{\nu} + \mathbf{D}\boldsymbol{\nu} + \mathbf{d}_n(\boldsymbol{\Theta},\boldsymbol{\nu}) + \boldsymbol{\mu} + \mathbf{g}(\boldsymbol{\eta}) = \boldsymbol{\tau}_{\text{env}} + \boldsymbol{\tau} \tag{138}$$

$$\dot{\boldsymbol{\chi}} = \mathbf{A}_r\boldsymbol{\chi} + \mathbf{B}_r\delta\boldsymbol{\nu}, \qquad \boldsymbol{\chi}(0) = \mathbf{0} \tag{139}$$

$$\boldsymbol{\mu} = \mathbf{C}_r\boldsymbol{\chi} + \mathbf{D}_r\delta\boldsymbol{\nu} \tag{140}$$

Notice that the property:

$$\mathbf{M} = \mathbf{M}^\top > 0, \qquad \dot{\mathbf{M}} = \mathbf{0} \tag{141}$$

holds for this model since the generalized added mass matrix $\tilde{\mathbf{M}}_A(\infty)$ is frequency independent and symmetric. Hence, Lyapunov-based control methods [Fossen, 2002] can utilize the standard kinetic energy formulation:

$$V(\boldsymbol{\nu}) = \frac{1}{2}\boldsymbol{\nu}^\top\mathbf{M}\boldsymbol{\nu} > 0, \quad \forall\boldsymbol{\nu} \neq \mathbf{0} \tag{142}$$

6.2 Zero-Speed State-Space Representation

An attractive simplification of (137)–(140) is the DP representation which is obtained for $U = 0$ and $\omega_e = \omega$. Hence, $\mathbf{C}_{RB}\boldsymbol{\nu} = \mathbf{0}, \tilde{\mathbf{C}}_A(\omega)\boldsymbol{\nu} = \mathbf{0}, \mathbf{d}(\boldsymbol{\Theta}, \boldsymbol{\nu})$ is small, and $\mathbf{g}(\boldsymbol{\eta}) \approx \mathbf{G}\boldsymbol{\eta}$, such that [Fossen and Smogeli, 2004]:

$$\mathbf{M}\dot{\boldsymbol{\nu}} + \mathbf{D}\boldsymbol{\nu} + \int_0^t \mathbf{K}(t-\tau)\boldsymbol{\nu}(\tau)d\tau + \mathbf{G}\boldsymbol{\eta} = \boldsymbol{\tau}_{\text{env}} + \boldsymbol{\tau} \tag{143}$$

where:

$$\begin{aligned} \mathbf{K}(t) &= \frac{2}{\pi}\int_0^\infty \mathbf{J}^{*\top}(\mathbf{B}(\omega) - \mathbf{B}(\infty))\mathbf{J}^* \cos(\omega t)d\omega \\ \mathbf{M} &= \mathbf{M}_{RB} + \mathbf{J}^{*\top}\mathbf{A}(\infty)\mathbf{J}^* \\ \mathbf{D} &= \mathbf{J}^{*\top}\mathbf{B}(\infty)\mathbf{J}^* \end{aligned}$$

The state-space model now becomes:

$$\dot{\boldsymbol{\eta}} = \mathbf{J}(\boldsymbol{\Theta})\boldsymbol{\nu} \tag{144}$$

$$\mathbf{M}\dot{\boldsymbol{\nu}} + \mathbf{D}\boldsymbol{\nu} + \boldsymbol{\mu} + \mathbf{G}\boldsymbol{\eta} = \boldsymbol{\tau}_{\text{env}} + \boldsymbol{\tau} \tag{145}$$

$$\dot{\boldsymbol{\chi}} = \mathbf{A}_r\boldsymbol{\chi} + \mathbf{B}_r\boldsymbol{\nu} \tag{146}$$

$$\boldsymbol{\mu} = \mathbf{C}_r\boldsymbol{\chi} + \mathbf{D}_r\boldsymbol{\nu} \tag{147}$$

where $\boldsymbol{\chi}(0) = \mathbf{0}$.

7 Strip Theory

This section presents a method for transformation of the STF hydrodynamic coefficients [Salvesen *et al.*, 1970] used in the unified model of Section 5.

7.1 Background

In 1949 Ursell published his famous paper on potential theory for determining the hydrodynamic coefficients of semi-circular cross sections, oscillating in deep water in the frequency domain [Ursell, 1949]. This was used as a rough estimation for zero speed ship applications. Motivated by this Grim [1953], Tasai (1959, 1960, 1961), Gerritsma [1960] and others used conformal mapping techniques like the Lewis conformal mapping to transform ship-like cross sections to semicircles such that more realistic hull forms could be calculated. Exciting wave loads were computed using undisturbed regular waves. Denis and Pierson [1953] published a superposition method to describe the irregular waves assuming that the sea could be described as a sum of many simple harmonic waves; each wave with its own frequency, amplitude, direction and random phase lag. The responses of the ship at zero speed were calculated for each of these individual harmonic waves and superimposed.

The extension to forward speed was made available by Korvin-Kroukovsky and Jacobs [1957], and was further improved in the 60s. Later, Frank [1967] published a pulsating source theory to calculate the hydrodynamic coefficients of a cross section of a ship in deep water directly, without using conformal mapping. Keil [1974] published a theory for obtaining the potential coefficients in very shallow water using Lewis conformal mappings. The STF strip theory [Salvesen *et al.*, 1970], which accounts for forward speed as well as transom stern effects, is made available through the program ShipX (VERES) [Fathi and Hoff, 2004].

Since strip theory determines the hydrodynamic coefficients from potential theory, it is common to calculate the added resistance of a ship due to waves e.g. by using the integrated pressure method by Boese [1970] or the radiated energy method [Gerritsma and Beukelman, 1972]. In roll it is common to use the viscous correction by Ikeda *et al.* [1978] based on semi-empirical methods.

For zero-speed, 3-D potential theory can be used to compute the hydrodynamic coefficients [WAMIT, 2004], while the panel-method program T$_{\bar{1}}$MIT [Korsmeyer *et al.*, 1999] computes the impulse-response functions for different forward speeds. However, the 2-D approach (strip theory) is still very favorable for calculating the behavior of a ship at forward speed. For a more detailed discussion on advantages and disadvantages when comparing 2-D with 3-D theories; see Faltinsen and Svensen [1990].

7.2 Transformation of STF Coefficients

The STF strip theory coefficients of Salvesen *et al.* [1970] listed in Tables 3 and 4 in Appendix B should be transformed from the *h-frame* to the *b-frame* in order to implement the state-space model (137)–(140). This also removes the representation singularity at $\omega_e = 0$ caused by terms like U/ω_e^2 and U^2/ω_e^2.

Consider the *b-frame* frequency-dependent matrices:

$$\tilde{\mathbf{M}}_A(\omega_e) = \mathbf{J}^{*\top}\left[\mathbf{A}(\omega_e) - \frac{U}{\omega_e^2}\mathbf{B}(\omega_e)\mathbf{L}^*\right]\mathbf{J}^* \tag{148}$$

$$\tilde{\mathbf{N}}(\omega_e) = \mathbf{J}^{*\top}\left[\mathbf{B}(\omega_e) + U\mathbf{A}(\omega_e)\mathbf{L}^*\right]\mathbf{J}^* \tag{149}$$

Let the terms within the brackets be denoted as:

$$\mathbf{X}(\omega_e) = \mathbf{A}(\omega_e) - \frac{U}{\omega_e^2}\mathbf{B}(\omega_e)\mathbf{L}^* \quad (150)$$

$$\mathbf{Y}(\omega_e) = \mathbf{B}(\omega_e) + U\mathbf{A}(\omega_e)\mathbf{L}^* \quad (151)$$

such that:

$$\tilde{\mathbf{M}}_A(\omega_e) = \mathbf{J}^{*\top}\mathbf{X}(\omega_e)\mathbf{J}^* \quad (152)$$

$$\mathbf{Y}(\omega_e) = \mathbf{J}^{*\top}\mathbf{Y}(\omega_e)\mathbf{J}^* \quad (153)$$

Let us now consider the B_{55} coefficient in Table 3:

$$B_{55} = B_{55}^0 + \frac{U^2}{\omega_e^2}B_{33}^0 + Ux_A^2 a_{33}^A + \frac{U^2}{\omega_e^2}x_A b_{33}^A \quad (154)$$

which clearly is undefined for $\omega_e = 0$. However, the coefficient $\tilde{N}_{55}(\omega_e)$ with $\mathbf{J}^* = \mathbf{I}$ is well conditioned since:

$$\begin{aligned}\tilde{N}_{55} &= B_{55} - UA_{53} \\ &= B_{55}^0 + \frac{U^2}{\omega_e^2}B_{33}^0 + Ux_A^2 a_{33}^A + \frac{U^2}{\omega_e^2}x_A b_{33}^A \\ &\quad -U\left(A_{53}^o + \frac{U}{\omega_e^2}B_{33}^0 + \frac{U}{\omega_e^2}x_A b_{33}^A\right) \\ &= B_{55}^0 - UA_{53}^0 + Ux_A^2 a_{33}^A \end{aligned} \quad (155)$$

This also holds for the other coefficients. Inspired by this, a systematic transformation procedure is presented below.

7.3 Longitudinal and Lateral Transformations

The transformation matrix $\mathbf{J}^*$ given by (86) can be partitioned according to:

$$\mathbf{J}_1^* = \begin{bmatrix} 1 & 0 & z_w \\ 0 & 1 & -x_w \\ 0 & 0 & 1 \end{bmatrix} \quad (156)$$

$$\mathbf{J}_2^* = \begin{bmatrix} 1 & -z_w & x_w \\ 0 & 1 & 0 \\ 0 & 0 & 1 \end{bmatrix} \quad (157)$$

for the *longitudinal* and *lateral modes*, respectively. At the infinity frequency we have that:

$$\begin{aligned}\tilde{\mathbf{M}}_A(\infty) &= \mathbf{J}^{*\top}\mathbf{A}(\infty)\mathbf{J}^* \\ \tilde{\mathbf{N}}(\infty) &= \mathbf{J}^{*\top}\left[\mathbf{B}(\infty) + U\mathbf{A}(\infty)\mathbf{L}^*\right]\mathbf{J}^*\end{aligned}$$

which both are constant matrices. The $\mathbf{Y}(\omega_e)$ matrix is:

$$\begin{aligned}&\mathbf{Y}(\omega_e) = \mathbf{B}(\omega_e) + U\mathbf{A}(\omega_e)\mathbf{L}^* \\ &= \begin{bmatrix} B_{11} & 0 & B_{13} & 0 & B_{15}-UA_{13} & 0 \\ 0 & B_{22} & 0 & B_{24} & 0 & B_{26}+UA_{22} \\ B_{31} & 0 & B_{33} & 0 & B_{35}-UA_{33} & 0 \\ 0 & B_{42} & 0 & B_{44} & 0 & B_{46}+UA_{42} \\ B_{51} & 0 & B_{53} & 0 & B_{55}-UA_{53} & 0 \\ 0 & B_{62} & 0 & B_{64} & 0 & B_{66}+UA_{62} \end{bmatrix}\end{aligned}$$

Substituting the STF coefficients from Table 3 into the expression for $\mathbf{Y}(\omega_e)$ gives the following *longitudinal transformation*:

$$\begin{aligned}&\begin{bmatrix} Y_{11} & Y_{13} & Y_{15} \\ Y_{31} & Y_{33} & Y_{35} \\ Y_{51} & Y_{53} & Y_{55} \end{bmatrix} \\ &= \begin{bmatrix} B_{11}^0 & B_{13}^0 & B_{15}^0 \\ B_{31}^0 & B_{33}^0+Ua_{33}^A & B_{33}^0-Ux_A a_{33}^A \\ B_{51}^0 & B_{53}^0-UA_{33}^0-Ux_A a_{33}^A & B_{55}^0-UA_{53}^0+Ux_A^2 a_{33}^A \end{bmatrix}\end{aligned}$$

and

$$\begin{bmatrix} \tilde{N}_{11} & \tilde{N}_{13} & \tilde{N}_{15} \\ \tilde{N}_{31} & \tilde{N}_{33} & \tilde{N}_{35} \\ \tilde{N}_{51} & \tilde{N}_{53} & \tilde{N}_{55} \end{bmatrix} = \mathbf{J}_1^{*\top}\begin{bmatrix} Y_{11} & Y_{13} & Y_{15} \\ Y_{31} & Y_{33} & Y_{35} \\ Y_{51} & Y_{53} & Y_{55} \end{bmatrix}\mathbf{J}_1^* \quad (158)$$

The *lateral transformation* corresponding to Table 4 is:

$$\begin{aligned}&\begin{bmatrix} Y_{22} & Y_{24} & Y_{26} \\ Y_{42} & Y_{44} & Y_{46} \\ Y_{62} & Y_{64} & Y_{66} \end{bmatrix} \\ &= \begin{bmatrix} B_{22}^0+Ua_{22}^A & B_{24}^0+Ua_{24}^A & B_{26}^0+Ux_A a_{22}^A \\ B_{42}^0+Ua_{24}^A & B_{44}^0+Ua_{44}^A+B_{44}^* & B_{24}^0+Ux_A a_{24}^A \\ B_{62}^0+UA_{22}^0+Ux_A a_{22}^A & B_{64}^0+UA_{24}^0+Ux_A a_{24}^A & B_{66}^0+Ux_A^2 a_{22}^A+UA_{62}^0 \end{bmatrix}\end{aligned}$$

and

$$\begin{bmatrix} \tilde{N}_{22} & \tilde{N}_{24} & \tilde{N}_{26} \\ \tilde{N}_{42} & \tilde{N}_{44} & \tilde{N}_{46} \\ \tilde{N}_{62} & \tilde{N}_{64} & \tilde{N}_{66} \end{bmatrix} = \mathbf{J}_2^{*\top}\begin{bmatrix} Y_{22} & Y_{24} & Y_{26} \\ Y_{42} & Y_{44} & Y_{46} \\ Y_{62} & Y_{64} & Y_{66} \end{bmatrix}\mathbf{J}_2^* \quad (159)$$

Notice that all singular points due to the terms U/ω_e^2 and U^2/ω_e^2 now have been removed.

8 Relationship between Maneuvering and Seakeeping Theory

In Section 5 the *unified model* was derived in the *b-frame* using seakeeping theory and nonlinear damping terms. This is highly advantageous since the resulting model incorporates the maneuvering equations as a special case.

The unified model is related to classical maneuvering theory by neglecting the memory effect of the fluid i.e. only considering the static terms corresponding to the zero frequency. This is illustrated below.

Figure 9: Maneuvering of a tanker in calm water. For this case $\omega_e = 0$ is a good approximation.

Figure 10: Maneuvering in a seaway. For this case $\omega_e = 0$ is a cruel approximation (Courtesy Maersk).

8.1 LF and WF Models

In maneuvering theory the low-frequency assumption:

$$\omega_e = 0 \tag{160}$$

implies that the motions can be separated into LF and WF motion components. The zero-frequency model is:

$$\dot{\boldsymbol{\eta}}_{LF} = \mathbf{J}(\boldsymbol{\Theta}_{LF})\boldsymbol{\nu}_{LF} \tag{161}$$

$$\begin{aligned}[\mathbf{M}_{RB} + \mathbf{M}_A]\,\dot{\boldsymbol{\nu}}_{LF} + \mathbf{C}_{RB}\boldsymbol{\nu}_{LF} + \mathbf{N}\boldsymbol{\nu}_{LF} \\ + \mathbf{d}_n(\boldsymbol{\Theta}_{LF}, \boldsymbol{\nu}_{LF}) + \mathbf{g}(\boldsymbol{\eta}_{LF}) = \boldsymbol{\tau}_{\rm env} + \boldsymbol{\tau}\end{aligned} \tag{162}$$

where the *oscillatory derivatives* $\tilde{\mathbf{M}}_A(\omega_e)$ and $\tilde{\mathbf{N}}(\omega_e)$ are evaluated at $\omega_e = 0$, that is:

$$\mathbf{M}_A = \tilde{\mathbf{M}}_A(0) \tag{163}$$

$$\mathbf{N} = \tilde{\mathbf{N}}(0) \tag{164}$$

Note that $\boldsymbol{\tau}_{\rm env}$ for $\boldsymbol{\tau}_{\rm FK+diff} = \mathbf{0}$ reduces to:

$$\boldsymbol{\tau}_{\rm env} = \boldsymbol{\tau}_{\rm drift} + \boldsymbol{\tau}_{\rm wind} + \boldsymbol{\tau}_{\rm currents} \tag{165}$$

This is done under the assumption that the WF motions due to $\boldsymbol{\tau}_{\rm FK+diff}$ can be added directly to the output as two signals $\boldsymbol{\eta}_{WF}$ and $\boldsymbol{\nu}_{WF}$, that is:

$$\boldsymbol{\eta} = \boldsymbol{\eta}_{LF} + \boldsymbol{\eta}_{WF} \tag{166}$$

$$\boldsymbol{\nu} = \boldsymbol{\nu}_{LF} + \boldsymbol{\nu}_{WF} \tag{167}$$

Figure 9 shows a ship maneuvering in calm weather where $\omega_e = 0$ is a good assumption. In Figure 10 this assumption is clearly violated, suggesting that the unified model in Section 5 should be applied instead.

The hydrodynamic derivatives are defined in terms of the matrices $\mathbf{M}_A$ and $\mathbf{N}$ according to (see Section 5.1):

$$\begin{aligned}\mathbf{M}_A &= \mathbf{J}^{*\top}\mathbf{A}(0)\mathbf{J}^* - \lim_{\omega_e \to 0} \frac{U}{\omega_e^2}\mathbf{J}^{*\top}\mathbf{B}(\omega_e)\mathbf{L}^* \\ &= -\begin{bmatrix} X_{\dot{u}} & X_{\dot{v}} & X_{\dot{w}} & X_{\dot{p}} & X_{\dot{q}} & X_{\dot{r}} \\ Y_{\dot{u}} & Y_{\dot{v}} & Y_{\dot{w}} & Y_{\dot{p}} & Y_{\dot{q}} & Y_{\dot{r}} \\ Z_{\dot{u}} & Z_{\dot{v}} & Z_{\dot{w}} & Z_{\dot{p}} & Z_{\dot{q}} & Z_{\dot{r}} \\ K_{\dot{u}} & K_{\dot{v}} & K_{\dot{w}} & K_{\dot{p}} & K_{\dot{q}} & K_{\dot{r}} \\ M_{\dot{u}} & M_{\dot{v}} & M_{\dot{w}} & M_{\dot{p}} & M_{\dot{q}} & M_{\dot{r}} \\ N_{\dot{u}} & N_{\dot{v}} & N_{\dot{w}} & N_{\dot{p}} & N_{\dot{q}} & N_{\dot{r}} \end{bmatrix}\end{aligned}$$

$$\begin{aligned}\mathbf{N} &= \mathbf{J}^{*\top}\left[\mathbf{B}(0) + U\mathbf{A}(0)\mathbf{L}^*\right]\mathbf{J}^* \\ &= -\begin{bmatrix} X_u & X_v & X_w & X_p & X_q & X_r \\ Y_u & Y_v & Y_w & Y_p & Y_q & Y_r \\ Z_u & Z_v & Z_w & Z_p & Z_q & Z_r \\ K_u & K_v & K_w & K_p & K_q & K_r \\ M_u & M_v & M_w & M_p & M_q & M_r \\ N_u & N_{vp} & N_w & N_p & N_q & N_r \end{bmatrix}\end{aligned}$$

8.2 Decoupled Maneuvering Equations

The linear *longitudinal maneuvering equations* corresponding to (162) takes the following form (assuming that $\mathbf{g}(\boldsymbol{\eta}_{LF}) = \mathbf{G}\boldsymbol{\eta}_{LF}$ and $\mathbf{d}_n = \mathbf{0}$):

$$\begin{aligned}&\begin{bmatrix} m & 0 & 0 \\ 0 & m & 0 \\ 0 & 0 & I_y \end{bmatrix}\begin{bmatrix} \dot{u}_{LF} \\ \dot{w}_{LF} \\ \dot{q}_{LF} \end{bmatrix} + \begin{bmatrix} 0 & 0 & 0 \\ 0 & 0 & -mU \\ 0 & 0 & 0 \end{bmatrix}\begin{bmatrix} u_{LF} \\ w_{LF} \\ q_{LF} \end{bmatrix} \\ &\quad - \begin{bmatrix} X_{\dot{u}} & X_{\dot{w}} & X_{\dot{q}} \\ Z_{\dot{u}} & Z_{\dot{w}} & Z_{\dot{q}} \\ M_{\dot{u}} & M_{\dot{w}} & M_{\dot{q}} \end{bmatrix}\begin{bmatrix} \dot{u}_{LF} \\ \dot{w}_{LF} \\ \dot{q}_{LF} \end{bmatrix} \\ &\quad - \begin{bmatrix} X_u & X_w & X_q \\ Z_u & Z_w & Z_q \\ M_u & M_w & M_q \end{bmatrix}\begin{bmatrix} u_{LF} \\ w_{LF} \\ q_{LF} \end{bmatrix} \\ &- \begin{bmatrix} 0 & 0 & 0 \\ 0 & Z_z & Z_\theta \\ 0 & M_z & M_\theta \end{bmatrix}\begin{bmatrix} x_{LF} \\ z_{LF} \\ \theta_{LF} \end{bmatrix} = \begin{bmatrix} \tau_{1,\rm env} \\ \tau_{3,\rm env} \\ \tau_{5,\rm env} \end{bmatrix} + \begin{bmatrix} \tau_1 \\ \tau_3 \\ \tau_5 \end{bmatrix}\end{aligned}$$

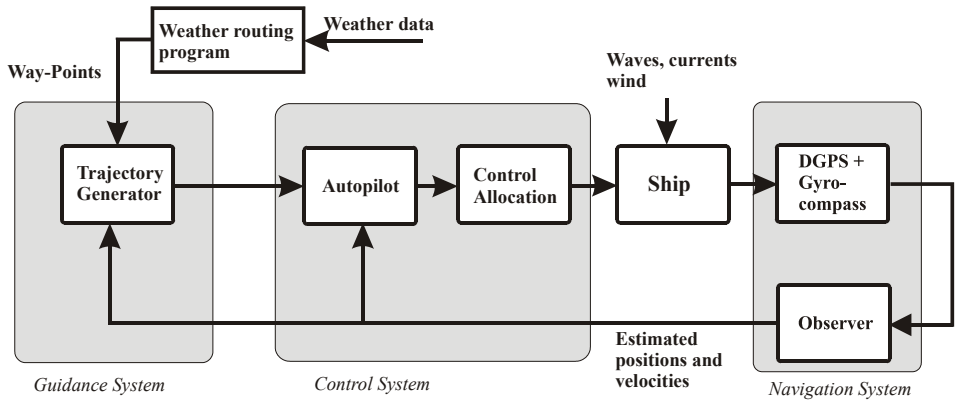

Figure 11: Interaction between the Guidance, Navigation, and Control blocks.

The *lateral maneuvering equations* takes the form:

$$\begin{bmatrix} m & 0 & 0 \\ 0 & I_x & -I_{xz} \\ 0 & -I_{xz} & I_z \end{bmatrix}\begin{bmatrix} \dot{v}_{LF} \\ \dot{p}_{LF} \\ \dot{r}_{LF} \end{bmatrix} + \begin{bmatrix} 0 & 0 & mU \\ 0 & 0 & 0 \\ 0 & 0 & 0 \end{bmatrix}\begin{bmatrix} v_{LF} \\ p_{LF} \\ r_{LF} \end{bmatrix} - \begin{bmatrix} Y_{\dot{v}} & Y_{\dot{p}} & Y_{\dot{r}} \\ K_{\dot{v}} & K_{\dot{p}} & K_{\dot{r}} \\ N_{\dot{v}} & N_{\dot{p}} & N_{\dot{r}} \end{bmatrix}\begin{bmatrix} \dot{v}_{LF} \\ \dot{p}_{LF} \\ \dot{r}_{LF} \end{bmatrix} - \begin{bmatrix} Y_v & Y_p & Y_r \\ K_v & K_p & K_r \\ N_{vp} & N_p & N_r \end{bmatrix}\begin{bmatrix} v_{LF} \\ p_{LF} \\ r_{LF} \end{bmatrix} - \begin{bmatrix} 0 & 0 & 0 \\ 0 & K_\phi & 0 \\ 0 & 0 & 0 \end{bmatrix}\begin{bmatrix} y_{LF} \\ \phi_{LF} \\ \psi_{LF} \end{bmatrix} = \begin{bmatrix} \tau_{2,\text{env}} \\ \tau_{4,\text{env}} \\ \tau_{6,\text{env}} \end{bmatrix} + \begin{bmatrix} \tau_2 \\ \tau_4 \\ \tau_6 \end{bmatrix}$$

9 The History of Model-Based Ship Control

This section briefly describes the history of the gyroscope and how it contributed to the development of the first automatic ship steering mechanism in 1911 to the fully automated systems of today based on gyro compasses and global satellite navigation systems.

9.1 The Gyroscope and its Contributions to Ship Control

In 1851 Léon Foucault, a French physicist, demonstrated the Earth's rotation by showing that a pendulum continued to swing in the same plane while the Earth turned around. This inspired him to invent the gyroscope the next year. He named the device from the Greek words gyros, "revolution," and skopein, "to view" because he used it to "view the Earth's rotation."

However, the first recorded construction of the gyroscope is usually credited to Bohnenberger in 1810 who used a heavy ball instead of a wheel. Unfortunately, this faded into history since it had no scientific application. 80 years later Hopkins demonstrated the first electrically driven gyroscope. The development of the electrically driven gyroscope was motivated by the need of more reliable navigation systems for steel ships and underwater warfare (magnetic compasses are sensitive for magnetic disturbances), [see Allensworth, 1999; Bennet, 1979].

In parallel works, Anschutz and Sperry both worked on a practical application of the gyroscope. In 1908 Anschutz patented the first North seeking gyrocompass while Sperry was granted a patent for his ballistic compass in 1911.

9.2 Model-Based Ship Control

The invention of gyroscope was one of the breakthroughs in automatic ship control since it gave reliable heading measurements ψ. The gyro together with linear accelerometers are also the key components of a vertical reference unit (VRU) which measures the roll and pitch angles (ϕ, θ). Today, global satellite navigation systems have further extended the possibilities for automatic control and terrestrial navigation of ships since they provide the user with the North-East-Down positions (n, e, d).

A marine vessel control system is usually constructed as three independent blocks denoted as the guidance, navigation and control (GNC) systems. These systems interact with each other through data and signal transmission as illustrated in Figure 11 where a conventional ship autopilot is shown.

GNC, in its most basic form, is a reference model

(guidance system), a sensor system (navigation system) and a feedback control system. In its most advanced form, the GNC blocks represent three interconnected subsystems [Fossen, 2002]:

Guidance is the action or the system that continuously computes the reference (desired) position, velocity and acceleration of a vessel to be used by the control system. These data are usually provided to the human operator and the navigation system. The basic components of a guidance system are motion sensors, external data like weather data (wind speed and direction, wave height and slope, current speed and direction, etc.) and a computer. The computer collects and processes the information, and then feeds the results to the vessel's control system. In many cases, advanced optimization techniques are used to compute the optimal trajectory or path for the vessel to follow. This might include sophisticated features like fuel optimization, minimum time navigation, weather routing, collision avoidance, formation control and schedule meetings.

Navigation is the science of directing a craft by determining its position, course, and distance traveled. In some cases velocity and acceleration are determined as well. This is usually done by using a satellite navigation system combined with motion sensors like accelerometers and gyros. The most advanced navigation system for marine applications is the *inertial navigation system* (INS). Navigation is derived from the Latin *navis*, "ship," and *agere*, "to drive." It originally denoted the art of ship driving, including steering and setting the sails. The skill is even more ancient than the word itself, and it has evolved over the course of many centuries into a technological science that encompasses the planning and execution of safe, timely, and economical operation of ships, underwater vehicles, aircraft, and spacecraft.

Control is the action of determining the necessary control forces and moments to be provided by the vessel in order to satisfy a certain *control objective.* The desired control objective is usually seen in conjunction with the guidance system. Examples of control objectives are minimum energy, set-point regulation, trajectory tracking, path following, maneuvering etc. Constructing the control algorithm involves the design of feedback and feedforward control laws. The outputs from the navigation system, position, velocity and acceleration, are used for feedback control while feedforward control is implemented using signals available in the guidance system and other external sensors.

In the forthcoming sections, we will focus on the:

- Classical 1 DOF autopilot design for heading (*yaw*) control
- Extensions to 3 DOF (*surge, sway*, and *yaw*) maneuvering and station-keeping (dynamic positioning)

The modelling techniques presented in this paper can also be extended to rudder-roll damping and fin stabilization using models in 4 DOF (*surge, sway, roll,* and *yaw*) [Perez, 2005] as well as the general motion in 6 DOF.

9.3 Process Plant and Control Plant Models

When designing model-based ship control systems it is important to distinguish between the *control plant* and *process plant* models. The following definitions are adopted from Sørensen [2005]:

Control Plant Model is a simplified mathematical description containing only the main physical properties of the process or plant. This model may constitute a part of the controller. The control plant model is also used in analytical stability analysis using e.g. eigenvalues, Lyapunov stability, or passivity.

Process Plant Model is a comprehensive description of the actual process and it should be as detailed as needed. The main purpose of this model is to simulate the real plant dynamics. The process plant model is used in numerical performance and robustness analyses, and testing of the control systems.

10 Heading Autopilot Systems

In this section, we describe the models for autopilot design and the construction of conventional model-based autopilot systems.

10.1 Classical Autopilot (LF Model)

The most common model used in heading autopilot systems is the well celebrated *Nomoto model* [Nomoto *et al.*, 1957], which can be derived from the *maneuvering model*:

$$\dot{\psi}_{LF} = r_{LF} \tag{168}$$

$$\begin{aligned}(I_z - N_{\dot{r}})\dot{r}_{LF} - N_r r_{LF} &= \tau_{\rm N} \\ &= \tau_{\rm rudder} + \tau_{\rm wind}\end{aligned} \tag{169}$$

where $-N_{\dot{r}} > 0$ and $-N_r > 0$ are the hydrodynamic derivatives, r_{LF} and ψ_{LF} are the LF yaw rate and yaw angle, $\tau_{\rm wind}$ is the wind moment, and $\tau_{\rm rudder}$ is the control input (yaw moment).

If wind speed and direction are measured, $\tau_{\rm wind}$ can be estimated using wind coefficient tables.

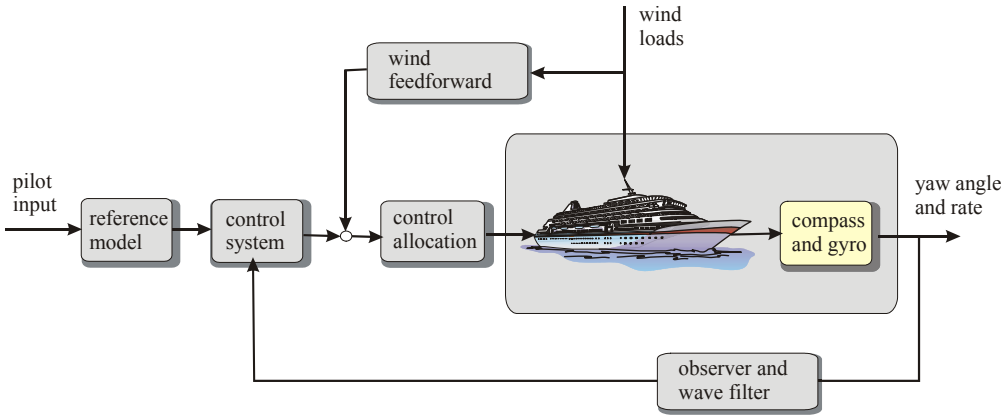

Figure 11: Block diagram showing a conventional autopilot system [Fossen, 2002].

Then the rudder command is computed from the feedback signal $\tau_{\rm N}$ and the feedforward signal $\tau_{\rm wind}$ as:

$$\tau_{\rm rudder} = \tau_{\rm N} - \tau_{\rm wind} \tag{170}$$

The Nomoto time constant T and gain constant K for this model can be defined as:

$$T \triangleq \frac{I_z - N_{\dot{r}}}{-N_r}, \quad K \triangleq \frac{1}{-N_r} \tag{171}$$

This gives:

$$\begin{aligned} \dot{\psi}_{LF} &= r_{LF} && (172)\\ T\dot{r}_{LF} + r_{LF} &= K\tau_{\rm N} && (173)\\ \psi &= \psi_{LF} + \psi_{WF} && (174) \end{aligned}$$

where motion due to 1st-order wave loads are added directly to the output.

The wave-induced motions ψ_{WF} are computed using the RAO transfer function:

$$RAO(s, \psi_r) = \frac{\psi_{WF}(s, \psi_r)}{\zeta_a} \tag{175}$$

For certain ships like large tankers it is necessary to add a nonlinear maneuvering characteristic. Again a zero-frequency assumption is used. A frequently used nonlinear model is [Norrbin, 1963]:

$$T\dot{r}_{LF} + r_{LF} + \alpha K r_{LF}^3 = K\tau_{\rm N} \tag{176}$$

where $\alpha > 0$ describes the nonlinear maneuvering characteristic.

10.2 Frequency-Dependent Autopilot Model

The *frequency-dependent model* (seakeeping theory) is:

$$[I_z + \tilde{M}_{A66}(\omega_e)]\dot{r} + \tilde{N}_{66}(\omega_e) r = \tau_{\rm N} \tag{177}$$

which relates to maneuvering theory ($\omega_e = 0$) according to:

$$\begin{aligned} -N_{\dot{r}} &\triangleq \tilde{M}_{A66}(0) && (178)\\ -N_r &\triangleq \tilde{N}_{66}(0) && (179) \end{aligned}$$

The *unified model* takes the form:

$$\dot{\psi} = r \tag{180}$$

$$\begin{aligned} &[I_z + \tilde{M}_{A66}(\infty)]\dot{r} + \tilde{N}_{66}(\infty) r \\ &\quad + \int_0^t K_{66}(t-\tau) r(\tau) d\tau + \alpha r^3 = \tau_{\rm env} + \tau_{\rm N} \end{aligned} \tag{181}$$

where the disturbance $\tau_{\rm env}$ represents wave loads due to Froude-Krylov forces, diffraction forces, and wave drift etc. Notice that we have added the nonlinear damper αr^3 directly to the time-domain equation (181). We have now extended the classical autopilot model (176) to describe different sea-states.

The integral term in (181) can be numerically computed e.g. by using trapezoidal integration. An alternative approach could be to approximate the impulse response:

$$\mu = \int_0^t K_{66}(t-\tau) r(\tau) d\tau \tag{182}$$

by a state-space model (A_r, B_r, C_r, D_r) [Kristiansen and Egeland, 2003]. Hence, we can write the unified autopilot model in state-space form as:

$$\dot{\psi} = r \tag{183}$$

$$\begin{aligned} &[I_z + \tilde{M}_{A66}(\infty)]\dot{r} \\ &\quad + \tilde{N}_{66}(\infty) r + \mu + \alpha r^3 = \tau_{\rm env} + \tau_{\rm N} \end{aligned} \tag{184}$$

$$\dot{\boldsymbol{\chi}} = \mathbf{A}_r\boldsymbol{\chi} + \mathbf{b}_r r, \quad \boldsymbol{\chi}(0) = \mathbf{0} \tag{185}$$
$$\mu = \mathbf{c}_r^\top \boldsymbol{\chi} + D_r r \tag{186}$$

The state-space model (185)–(186) will typically be of order 5 in order to approximate the impulse response (182) accurately. Hence, the autopilot model including the fluid memory effect is compactly represented as $2 + 5 = 7$ ODEs. The advantage of the model representation (183)–(186) to (172)–(174) is that it incorporates the memory effect of the fluid for varying sea states.

10.3 Autopilot Design

The autopilot systems of *Sperry* and *Minorsky* were both single-input single-output (SISO) control systems where the heading (yaw angle) of the ship was measured by a gyro compass. Today, this signal is fed back to a computer in which a PID-control system (autopilot) is implemented in software. The autopilot compares the operator set-point (desired heading) with the measured heading and computes the rudder command, which is then transmitted to the rudder servo for corrective action.

The main difference between the autopilot systems of Sperry and Minorsky and the modern autopilot is the increased functionality that has been added with sophisticated features like [Fossen, 2002]:

- Wave filtering; avoids 1st-order wave disturbances being fed back to the actuators.
- Adaptation to varying environmental conditions, shallow water effects and time-varying model parameters, e.g. changes in mass and centre of gravity.
- Wind feedforward for accurate and rapid course-changing maneuvers.
- Reference feedforward using a dynamic model, ψ_d, r_d, and $\dot{r}_d$, for course changing maneuvers. Course-keeping is obtained by using a constant reference signal, ψ_d = constant, as input to the reference model.

We will discuss some of these features more closely in the next sub-section.

10.3.1 Conventional Autopilot Design (Maneuvering Model)

Assume that both ψ and r are measured by using a compass and a rate gyro. A full state feedback PID-controller $\tau_{\rm N}$ for (172)–(174) can then be designed as [Fossen, 2002]:

$$\tau_{\rm N} = \tau_{\rm FF} - \frac{1}{K}[K_p\tilde{\psi} + \underbrace{K_pT_d}_{K_d}\tilde{r} + \underbrace{K_p/T_i}_{K_i}\int_0^t \tilde{\psi}(\tau)d\tau] \tag{187}$$

where $\tau_{\rm N}$ is the controller yaw moment, $\tau_{\rm FF}$ is a feedforward term to be determined, and

$$\tilde{\psi} = \psi_{LF} - \psi_d \tag{188}$$
$$\tilde{r} = r_{LF} - r_d \tag{189}$$

represent the yaw angle and yaw rate tracking errors for the reference signals ψ_d and r_d. The controller gains are:

$$K_p > 0 \quad \text{proportional gain constant}$$
$$T_d > 0 \quad \text{derivative time constant}$$
$$T_i > 0 \quad \text{integral time constant}$$

The controller gains can be found by pole placement, e.g. [Fossen 2002]:

$$K_p = T\omega_n^2$$
$$K_d = 2\zeta\omega_n T - 1$$
$$K_i = \frac{\omega_n}{10}K_p$$

where ζ is the desired relative damping ratio and ω_n is the desired natural frequency of the closed-loop system.

The feedforward term is chosen as:

$$\tau_{\rm FF} = \frac{T}{K}T\dot{r}_d + \frac{1}{K}r_d \tag{190}$$

The resulting error dynamics is:

$$T\dot{\tilde{r}} + (1 + K_d)\,\tilde{r} + K_p\tilde{\psi} + K_i\int_0^t \tilde{\psi}(\tau)d\tau = 0 \tag{191}$$

10.3.2 New Autopilot Design for the Unified Model

The conventional autopilot can be extended to include the memory effect of the fluid. This has not been tested in a practical design as far as the author knows, but it is straightforward to derive a pole-placement algorithm that incorporates the frequency-dependent terms of the model.

Consider the unified model (183)–(186) in the form:

$$\dot{\psi} = r \tag{192}$$
$$M\dot{r} + [D + D_{\rm mem}(s)]r + \alpha r^3 = \tau_{\rm env} + \tau_{\rm N} \tag{193}$$

where

$$M \triangleq I_z + \tilde{M}_{A66}(\infty) \tag{194}$$
$$D \triangleq \tilde{N}_{66}(\infty) \tag{195}$$

and the transfer function matrix $D_{\rm mem}(s)$ (memory effects) is:

$$D_{\rm mem}(s) \triangleq \mathbf{c}_r^\top(s\mathbf{I} - \mathbf{A}_r)^{-1}\mathbf{b}_r + D_r \tag{196}$$

This is done with a gentle abuse of notation since the signal $D_{\rm mem}(s)r$ must be implemented by filtering r using $D_{\rm mem}(s)$.

A nonlinear PID-controller with feedforward:

$$\begin{aligned}\tau_{\rm N} &= \tau_{\rm FF} + \alpha r^3 - K_p\tilde{\psi} - K_d\tilde{r} - K_i\int_0^t \tilde{\psi}(\tau)d\tau \\ \tau_{\rm FF} &= M\dot{r}_d + [D + D_{\rm mem}(s)]r_d \end{aligned} \quad (197)$$

now gives the error dynamics:

$$M\dot{\tilde{r}}+[D_{\rm mem}(s)+D+K_d]\tilde{r}+K_p\tilde{\psi}+K_i\int_0^t \tilde{\psi}(\tau)d\tau = \tau_{env} \quad (198)$$

which represents a stable system for proper tuning of K_p, K_d, and K_i.

11 Dynamic Positioning and Maneuvering Systems

Already in the 1960s three decoupled PID-controllers were applied to control the horizontal motion of ships (surge, sway and yaw) by means of thrusters and propellers. This was referred to as dynamic positioning (DP) systems. As for the autopilot systems, a challenging problem was to avoid that 1st-order wave-induced disturbances entered the feedback loop. Several techniques like notch and low-pass filtering and the use of dead-band techniques were tested for this purpose, but with different levels of success. In 1963 linear quadratic optimal controllers and the Kalman filter were published by Kalman and coauthors. This motivated the application of LQG-controllers in ship control since a state observer (Kalman filter) could be used to estimate the LF and WF motions. The LQG design technique was applied for this purpose by Balchen, Jenssen and Sælid (1976, 1980), and Grimble, Patton and Wise (1979, 1980). More lately, LQG control has been discussed by Sørensen *et al.* [1995]. Grimble and coauthors suggested to use $\mathcal{H}_\infty$ and μ-methods [Katebi *et al.*, 1997] for filtering and control in DP.

The control plant models for DP maneuvering systems will be classified according to the speed range in which the models are valid. Design of single model-based control system for DP and maneuvering at all speeds is currently an important field of research. This is the motivation for presenting the unified model of Section 5 since such a model can serve as basis for model-based control.

11.1 Speed Regimes

Strip theory programs can be applied on monohulls and catamarans at low as well as high speed. It is convenient to classify the models and speed regimes according to:

Low Speed $U \in [0, U_{DP}]$ *Dynamic positioning (station-keeping and low-speed maneuvering):* Low-speed maneuvering is typically defined by the speed range in which a linear speed independent hydrodynamic model is valid. Experience suggests that:

$$U_{DP} = 1.5 \text{ m/s} \approx 3 \text{ knots} \quad (199)$$

(1) For DP applications in the horizontal plane (*surge, sway,* and *yaw*), the LF ship model can be approximated by [Fossen and Strand, 1999]:

$$\begin{aligned}\dot{\boldsymbol{\eta}}_{LF} &= \mathbf{R}(\psi)\boldsymbol{\nu}_{LF} && (200)\\ \mathbf{M}\dot{\boldsymbol{\nu}}_{LF}+\mathbf{D}\boldsymbol{\nu}_{LF} + \mathbf{G}\boldsymbol{\eta}_{LF} &= \boldsymbol{\tau} + \mathbf{R}^\top(\psi)\mathbf{b} && (201)\\ \dot{\mathbf{b}} &= \mathbf{0} && (202)\end{aligned}$$

where

$$\mathbf{M}= \mathbf{M}_{RB} + \mathbf{J}^{*T}\mathbf{A}(0)\mathbf{J}^*, \quad \dot{\mathbf{M}} = \mathbf{0} \quad (203)$$

$$\mathbf{D}= \mathbf{J}^{*T}\mathbf{B}(0)\mathbf{J}^* \quad (204)$$

$\boldsymbol{\tau} = [\tau_1, \tau_2, \tau_6]^\top$ is the control input, $\boldsymbol{\nu}_{LF} = [u_{LF}, v_{LF}, r_{LF}]^\top$, $\boldsymbol{\eta}_{LF} = [n_{LF}, e_{LF}, \psi_{LF}]^\top$, and $\mathbf{b}$ is the *n*-frame bias due to currents. The WF model $\boldsymbol{\eta}_{WF} = [n_{WF}, e_{WF}, \psi_{WF}]^\top$ is computed using RAOs or three linear shaping filters:

$$\begin{aligned}n_{WF}(s) &= \frac{K_{w1}s}{s^2 + 2\lambda_1\omega_1 s + \omega_1^2}w_1(s) && (205)\\ e_{WF}(s) &= \frac{K_{w2}s}{s^2 + 2\lambda_2\omega_2 s + \omega_2^2}w_2(s) && (206)\\ \psi_{WF}(s) &= \frac{K_{w3}s}{s^2 + 2\lambda_3\omega_3 s + \omega_3^2}w_3(s) && (207)\end{aligned}$$

driven by the white noise terms $w_i(s)$ $(i = 1, 2, 3)$ such that the total motion becomes:

$$\boldsymbol{\eta} = \boldsymbol{\eta}_{LF} + \boldsymbol{\eta}_{WF} \quad (208)$$

(2) The unified DP model in a seaway can be written as, see Section 6.2:

$$\begin{aligned}\dot{\boldsymbol{\eta}} &= \mathbf{R}(\psi)\boldsymbol{\nu} && (209)\\ \mathbf{M}\dot{\boldsymbol{\nu}} + \mathbf{D}\boldsymbol{\nu} + \boldsymbol{\mu} + \mathbf{G}\boldsymbol{\eta} &= \boldsymbol{\tau} + \mathbf{R}^\top(\psi)\mathbf{b} && (210)\\ \dot{\mathbf{b}} &= \mathbf{0} && (211)\end{aligned}$$

where

$$\mathbf{M}= \mathbf{M}_{RB} + \mathbf{J}^{*T}\mathbf{A}(\infty)\mathbf{J}^*, \quad \dot{\mathbf{M}} = \mathbf{0} \quad (212)$$

$$\mathbf{D}= \mathbf{J}^{*T}\mathbf{B}(\infty)\mathbf{J}^* \quad (213)$$

Moderate Speed $U \in [U_{DP}, U_{\max}]$ *Maneuvering at moderate speeds:* The maximum speed depends on the Froude number:

$$F_n = \frac{U}{\sqrt{gL}} \quad (214)$$

where L is the length of the ship. The traditional strip theory, developed by Salvesen *et al.* [1970] , is valid up to $F_n = 0.25$–0.3. This suggests that:

$$U_{\max} = 0.3\sqrt{gL} \tag{215}$$

Hence, for a 80 m long supply vessel $U_{\max} = 8.4$ m/s.

(1) The LF maneuvering model is described in Section 8.
(2) The unified state-space model for this speed range is presented in Section 5.

High Speed $U > U_{\max}$ *High-speed maneuvering:* For high-speed craft lift theory must be taken into account. For *Froude numbers* $F_n \geq 0.4$, the high-speed formulation developed by Faltinsen and Zhao [1991a, 1991b] can be applied. In the Froude number range of 0.3–0.4, a comparison between the two methods should be carried out.

11.2 DP and Low-Speed Maneuvering Control System Design

The interested reader is recommended to consult Fossen [1994, 2002] and Perez [2005] for design methods and references on ship control systems design including DP, position mooring, autopilot design, way-point tracking, rudder-roll damping, fin stabilization, and maneuvering control.

The first book focuses on PID-control, pole-placement methods, and linear quadratic optimal control theory while the second book is dedicated to nonlinear control using Lyapunov methods. The third reference discusses autopilot design and combined fin stabilization and rudder-roll damping systems.

12 Case Study

The numerical computations for a zero-speed application using strip theory will now be presented. The S-175 container ship is used as case study. The main particulars of the S-175 container ship are given in Table 2.

Table 2: The S-175 main particulars

Ship	**S-175**
Length between perpendiculars (L_{pp})	175 m
Beam (B)	25.4 m
Draught (T)	9.5 m
Displaced volume (∇)	24,140 m^3
Block coefficient (c_B)	0.572
LCG relative to midships	-2.48 m
Froude number	0.25

12.1 Marine Systems Simulator (MSS)

The Marine Systems Simulator (MSS) [MSS, 2004] at the Norwegian University of Science and Technology can be used for time-domain simulation of ShipX (VERES) strip theory coefficients in Matlab/Simulink (see Section 7.2 and Appendix B).

In the MSS two Matlab m-files for postprocessing of the ShipX (VERES) data are provided. These are:

Veres2ABC.m	Computes the model matrices, retardation function, state-space models etc. Output file: *ABC.mat*
Veres2force.m	Creates a table of generalized diffraction/ Froude-Krylov force coefficients. Output file: *Forces_TF.dat*

The data flow is shown in Figure 13 where the S-175 container ship is used as case study.

Figure 13: Flow chart showing the numerical computations.

The data file *Forces_TF.dat* is used as input for the Simulink program *VeresFRC_DP.mdl* while the file *ABC.mat* must be manually loaded into work space. The numerical recipes used in the postprocessing of the data are described in Fossen and Smogeli [2004].

The frequency-dependent added mass and potential damping coefficients including viscous effects are shown in Figure 15. Time series of hydrodynamic excitation forces are shown in Figure 16. The retardation functions are given in Figure 14. The numerical results are computed for beam seas with the JONSWAP wave spectrum using significant wave height $H_{1/3} = 5$ m and peak frequency $\omega_p = 0.56$ rad/s. The wave spreading factor was set to 4.

13 Conclusions

A unified state-space model for ship maneuvering, station-keeping, and control in a seaway has been presented in a vectorial setting using state-space models. A transformation procedure for the STF strip theory coefficients has been developed by formulating the time-domain equations of motion in the body-fixed reference frame instead of the equilibrium or hydrodynamic reference frame.

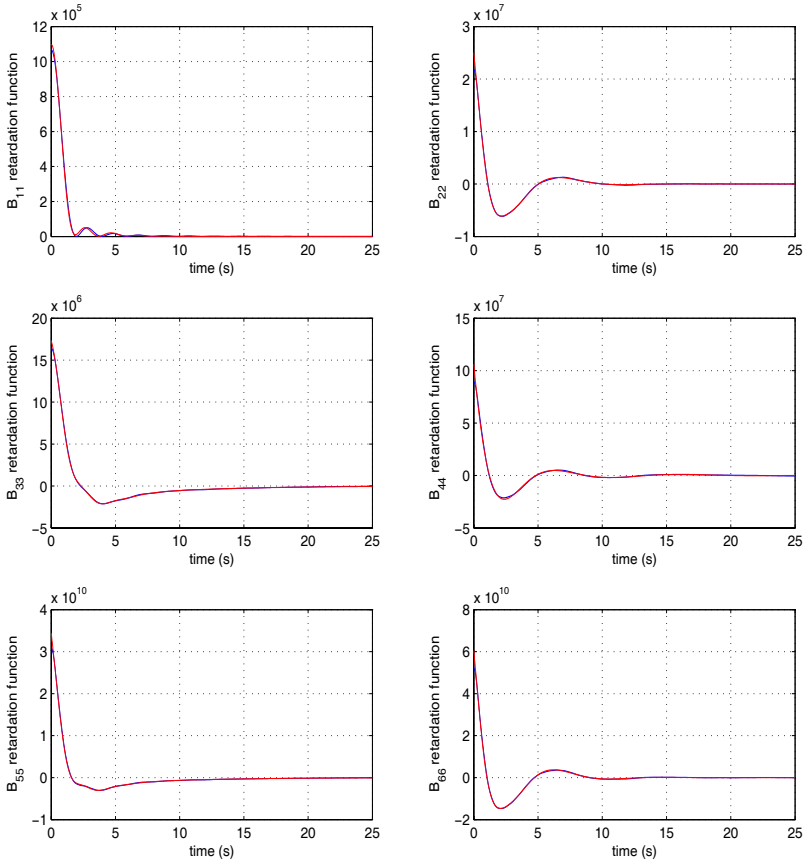

Figure 13: The retardation functions K_{ii} are computed from (227) using trapezoidal integrations and plotted as a function of time t. The corresponding state-space models (5th-order) are plotted on top.

By doing this ill-conditioned terms like U/ω_e^2 and U^2/ω_e^2, which are undefined for $\omega_e = 0$, are avoided when computing the retardation functions. This gives excellent numerical properties for $U \geq 0$. The developed procedure has been motivated by the results of Bishop and Price [1981] and Bailey *et al.* [1998].

The unified model can be used to simulate ships and rigs in a seaway for varying sea states and at different speeds (including zero speed). The model is valid up to *Froude numbers* 0.25–0.3 which are the upper limit for conventional strip theory programs like ShipX (VERES) and SEAWAY. The unified model can also be related to the zero-frequency maneuvering model and it is possible to include nonlinear maneuvering terms by unifying the theories of seakeeping and maneuvering.

Acknowledgment

This project is sponsored by the Centre for Ships and Ocean Structures, NTNU, through The Research Council of Norway.

The author is grateful to Øyvind N. Smogeli, Erlend Kristiansen, Dr. Tristan Perez, Professor Odd Faltinsen, and Professor Olav Egeland for valuable discussions and proof reading.

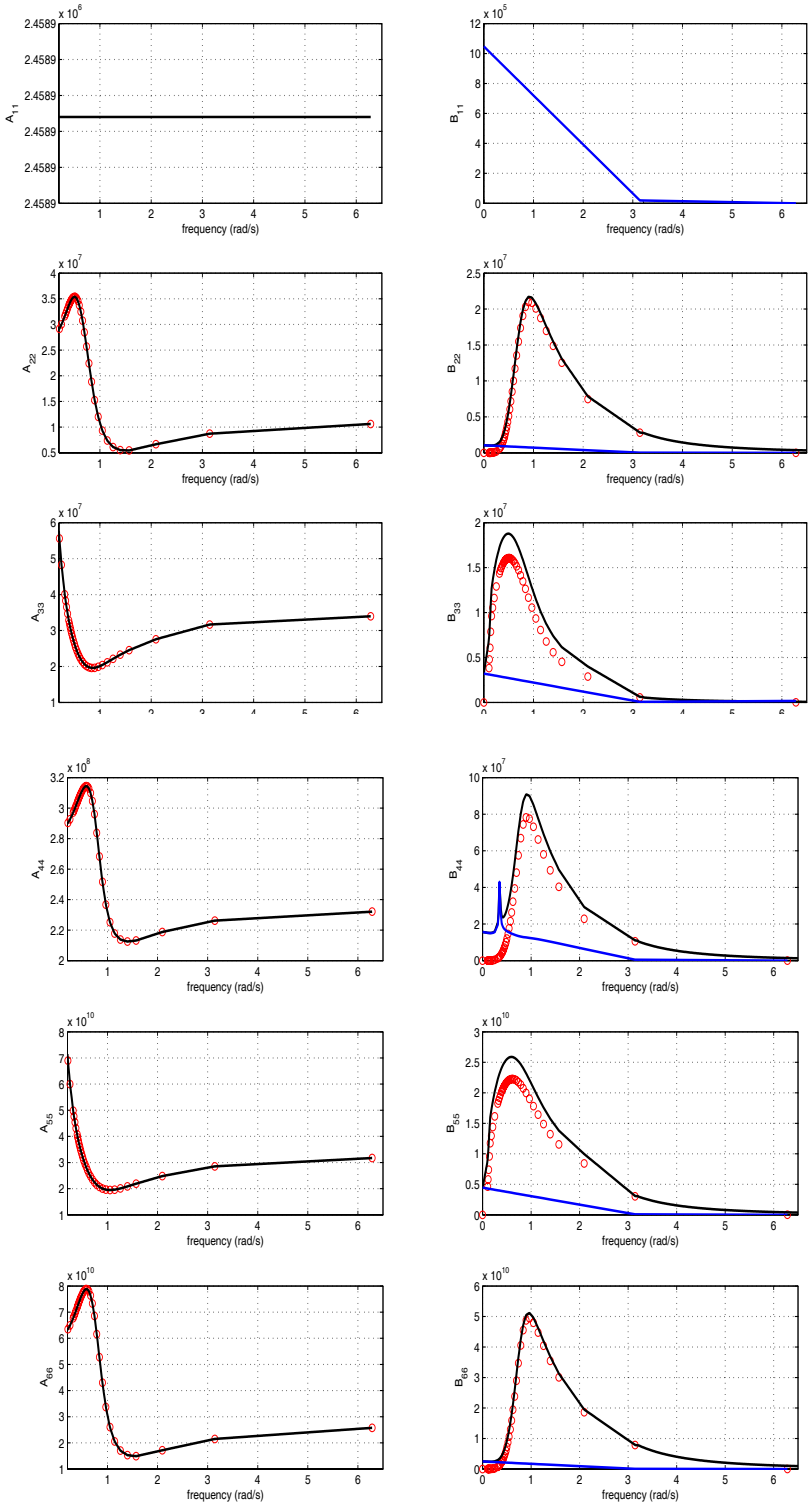

Figure 15: Frequency-dependent added mass A_{ii} and damping B_{ii} $(i = 1...6)$ for the S-175 container ship. Circles indicates VERES data points while the solid line is due to interpolation. For the B_{ii}-data, the high-frequency approximation β_{ii}/ω^3 is applied. In addition, a viscous ramp function is added to the B_{ii}-plots. For surge, added mass A_{11} is chosen as 10% of the mass while B_{11} simply is a viscous ramp. Added resistance data can further be used to improve damping in surge. For roll, the viscous effect to due bilge keels (and possible anti-roll tanks) is included in the B_{44}-plot.

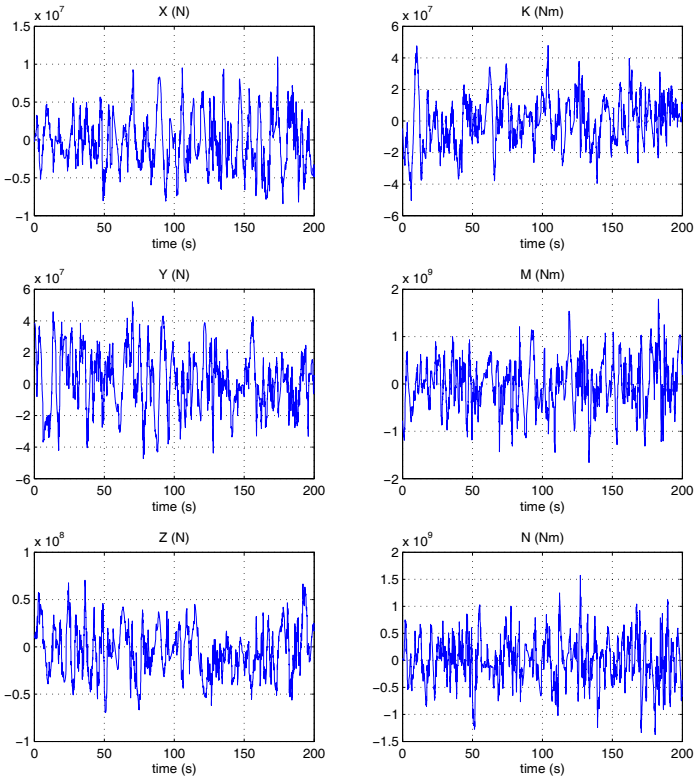

Figure 16: Diffraction and Froude-Krylov forces and moments in 6 DOF versus time, simulated in Simulink using VERES data tables.

A Cummins Equation

The hydromechanical reaction forces and moments, due to time-varying ship motions, can be described using Cummins [1962] formulation. From potential theory he showed that a rigid-body with generalized inertia matrix $\mathbf{M}^*_{RB}$ satisfies:

$$\mathbf{M}^*_{RB}\delta\ddot{\boldsymbol{\eta}}^* = \delta\boldsymbol{\tau}^*_H + \delta\boldsymbol{\tau}^* \tag{216}$$

where $\delta\boldsymbol{\tau}^*$ is the generalized external force vector and $\delta\boldsymbol{\tau}^*_H$ is the hydrodynamic generalized force vector:

$$\delta\boldsymbol{\tau}^*_H = -\bar{\mathbf{A}}^*\delta\ddot{\boldsymbol{\eta}}^* - \int_{-\infty}^{t} \bar{\mathbf{K}}^*(t-\tau)\delta\dot{\boldsymbol{\eta}}^*(\tau)d\tau - \bar{\mathbf{C}}^*\delta\boldsymbol{\eta}^* \tag{217}$$

in which $\bar{\mathbf{A}}^*$ is the generalized hydrodynamic added mass matrix, $\bar{\mathbf{C}}^*$ is the spring stiffness matrix, and $\bar{\mathbf{K}}^*(t-\tau)$ is a matrix of retardation functions. In honor of his work the *time-domain equation*:

$$[\mathbf{M}^*_{RB}+\bar{\mathbf{A}}^*]\delta\ddot{\boldsymbol{\eta}}^* + \int_{-\infty}^{t} \bar{\mathbf{K}}^*(t-\tau)\delta\dot{\boldsymbol{\eta}}^*(\tau)d\tau + \bar{\mathbf{C}}^*\delta\boldsymbol{\eta}^* = \delta\boldsymbol{\tau}^* \tag{218}$$

is referred to as *Cummins Equation.*

A.1 Relationship between the Time and Frequency Domain Equations

The coefficients $\bar{\mathbf{A}}^*$, $\bar{\mathbf{C}}^*$, and $\bar{\mathbf{K}}^*$ in Cummins equation can be determined by using the approach of Ogilvie [1964]. The classical *frequency domain* description used in computer programs based on potential theory starts with (99), i.e.:

$$[\mathbf{M}^*_{RB} + \mathbf{A}^*(\omega)]\delta\ddot{\boldsymbol{\eta}}^* + \mathbf{B}^*(\omega)\delta\dot{\boldsymbol{\eta}}^* + \mathbf{C}^*\delta\boldsymbol{\eta}^* = \delta\boldsymbol{\tau}^* \tag{219}$$

where the frequency-dependent hydrodynamic coefficient matrices $\mathbf{A}^*(\omega)$ and $\mathbf{B}^*(\omega)$ are due to added mass and po-

tential damping and $\delta\boldsymbol{\tau}^*$ is a vector of generalized excitation forces.

In Ogilvie [1964] it is assumed that the floating object carries out oscillations:

$$\delta\boldsymbol{\eta}^* = \cos(\omega t)\mathbf{I}_{6\times 6} \tag{220}$$

Substituting this expression into Cummins equation (218) gives:

$$-\omega^2[\mathbf{M}^*_{RB}+\bar{\mathbf{A}}^*]\cos(\omega t)+\omega\int_0^\infty \bar{\mathbf{K}}^*(\tau)\sin(\omega t-\omega\tau)d\tau + \bar{\mathbf{C}}^*\cos(\omega t) = \delta\boldsymbol{\tau}^*$$

where we have replaced τ by $t-\tau$ in the integral. This gives:

$$\begin{aligned}-\omega^2\left\{[\mathbf{M}^*_{RB}+\bar{\mathbf{A}}^*]-\frac{1}{\omega}\int_0^\infty \bar{\mathbf{K}}^*(\tau)\sin(\omega\tau)d\tau\right\}\cos(\omega t)\\ -\omega\left\{\int_0^\infty \bar{\mathbf{K}}^*(\tau)\cos(\omega\tau)d\tau\right\}\sin(\omega t)\\ +\bar{\mathbf{C}}^*\cos(\omega t) = \delta\boldsymbol{\tau}^*\end{aligned} \tag{221}$$

The classical model (219) gives:

$$\begin{aligned}-\omega^2\left\{[\mathbf{M}^*_{RB}+\mathbf{A}^*(\omega)\right\}\cos(\omega t)\\ -\omega\left\{\mathbf{B}^*(\omega)\sin(\omega\tau)d\tau\right\}\sin(\omega t)\\ +\mathbf{C}^*\cos(\omega t) = \delta\boldsymbol{\tau}^*\end{aligned} \tag{222}$$

By comparing the terms in (221) and (222), it is seen that:

$$\mathbf{A}^*(\omega) = \bar{\mathbf{A}}^* - \frac{1}{\omega}\int_0^\infty \bar{\mathbf{K}}^*(\tau)\sin(\omega\tau)d\tau \tag{223}$$

$$\mathbf{B}^*(\omega) = \int_0^\infty \bar{\mathbf{K}}^*(\tau)\cos(\omega\tau)d\tau \tag{224}$$

$$\mathbf{C}^* = \bar{\mathbf{C}}^* \tag{225}$$

The first equation must be valid for all ω. Hence, we choose to evaluate (223) at $\omega=\infty$ implying that:

$$\bar{\mathbf{A}}^* = \mathbf{A}^*(\infty) \tag{226}$$

The second equation is rewritten using the inverse Fourier transform giving:

$$\bar{\mathbf{K}}^*(t) = \frac{2}{\pi}\int_0^\infty \mathbf{B}^*(\omega)\cos(\omega\tau)d\omega \tag{227}$$

This expression is recognized as a matrix of *retardation functions*. Then, the relationship between the time-domain equation (218) and frequency-domain equation (219) has been established through:

$$\begin{aligned}&[\mathbf{M}^*_{RB}+\mathbf{A}^*(\infty)]\delta\ddot{\boldsymbol{\eta}}^*\\ &+\int_{-\infty}^t \bar{\mathbf{K}}^*(t-\tau)\delta\dot{\boldsymbol{\eta}}^*(\tau)d\tau + \mathbf{C}^*\delta\boldsymbol{\eta}^* = \delta\boldsymbol{\tau}^*\end{aligned} \tag{228}$$

A.2 Alternative Representation for Numerical Computations

From a numerical point of view is it better to integrate:

$$\mathbf{K}^*(t) = \frac{2}{\pi}\int_0^\infty [\mathbf{B}^*(\omega)-\mathbf{B}^*(\infty)]\cos(\omega\tau)d\omega \tag{229}$$

than to use (227), since $\mathbf{B}^*(\omega)-\mathbf{B}^*(\infty)$ is zero at $\omega=\infty$. Hence, we rewrite (228) as:

$$\begin{aligned}&[\mathbf{M}^*_{RB}+\mathbf{A}^*(\infty)]\delta\ddot{\boldsymbol{\eta}}^* + \mathbf{B}^*(\infty)\delta\dot{\boldsymbol{\eta}}^*\\ &+\int_{-\infty}^t \mathbf{K}^*(t-\tau)\delta\dot{\boldsymbol{\eta}}^*(\tau)d\tau + \mathbf{C}^*\delta\boldsymbol{\eta}^* = \delta\boldsymbol{\tau}^*\end{aligned}$$

This can be shown by writing (227) as:

$$\begin{aligned}\bar{\mathbf{K}}^*(t) &= \frac{2}{\pi}\int_0^\infty [\mathbf{B}^*(\omega)-\mathbf{B}^*(\infty)+\mathbf{B}^*(\infty)]\cos(\omega\tau)d\omega\\ &= \mathbf{K}^*(t)+\frac{2}{\pi}\int_0^\infty \mathbf{B}^*(\infty)\cos(\omega\tau)d\omega\end{aligned} \tag{230}$$

Hence:

$$\begin{aligned}&\int_{-\infty}^t \bar{\mathbf{K}}^*(t-\tau)\delta\dot{\boldsymbol{\eta}}^*(\tau)d\tau\\ &\quad=\int_{-\infty}^t \mathbf{K}^*(t-\tau)\delta\dot{\boldsymbol{\eta}}^*(\tau)d\tau + \mathbf{B}^*(\infty)\delta\dot{\boldsymbol{\eta}}^*\end{aligned} \tag{231}$$

since the inverse Fourier transform of the constant $\mathbf{B}^*(\infty)$ is an impulse. Moreover:

$$\mathbf{B}^*(\infty)\delta\dot{\boldsymbol{\eta}}^* = \int_{-\infty}^t\left(\frac{2}{\pi}\int_0^\infty \mathbf{B}^*(\infty)\cos(\omega\tau)d\omega\right)\delta\dot{\boldsymbol{\eta}}^*(\tau)d\tau \tag{232}$$

B STF Strip Theory

The STF strip theory coefficients can be decoupled into [Salvesen *et al.*, 1970]:

- Longitudinal modes (surge, heave, pitch)
- Lateral modes (sway, roll, yaw)

The longitudinal coefficients are given in Table 3 and the lateral coefficients in Table 4. The superscript 0 denotes speed independent terms.

Table 3: Longitudinal STF Strip Theory Coefficients

A_{11}	A^0_{11}
$A_{13}\ (= A_{31})$	A^0_{13}
B_{11}	B^0_{11}
$B_{13}\ (= B_{31})$	B^0_{13}
A_{15}	A^0_{15}
B_{15}	B^0_{15}
A_{51}	A^0_{51}
B_{51}	B^0_{51}
A_{33}	$A^0_{33} - \frac{U}{\omega_e^2} b^A_{33}$
B_{33}	$B^0_{33} + U a^A_{33}$
A_{35}	$A^0_{35} - \frac{U}{\omega_e^2} B^0_{33} + \frac{U}{\omega_e^2} x_A b^A_{33} - \frac{U^2}{\omega_e^2} a^A_{33}$
B_{35}	$B^0_{33} + U A^0_{33} - U x_A a^A_{33} - \frac{U^2}{\omega_e^2} b^A_{33}$
A_{53}	$A^o_{53} + \frac{U}{\omega_e^2} B^0_{33} + \frac{U}{\omega_e^2} x_A b^A_{33}$
B_{53}	$B^0_{53} - U A^0_{33} - U x_A a^A_{33}$
A_{55}	$A^0_{55} + \frac{U^2}{\omega_e^2} A^0_{33} - \frac{U}{\omega_e^2} x^2_A b^A_{33} + \frac{U^2}{\omega_e^2} x_A a^2_{33}$
B_{55}	$B^0_{55} + \frac{U^2}{\omega_e^2} B^0_{33} + U x^2_A a^A_{33} + \frac{U^2}{\omega_e^2} x_A b^A_{33}$

Table 4: Lateral STF Strip Theory Coefficients

A_{22}	$A^0_{22} - \frac{U}{\omega_e^2} b^A_{22}$
B_{22}	$B^0_{22} + U a^A_{22}$
$A_{24}\ (= A_{42})$	$A^0_{24} - \frac{U}{\omega_e^2} b^A_{24}$
$B_{24}\ (= B_{42})$	$B^0_{24} + U a^A_{24}$
A_{26}	$A^0_{26} + \frac{U}{\omega_e^2} B^0_{22} - \frac{U}{\omega_e^2} x_A b^A_{22} + \frac{U^2}{\omega_e^2} a^A_{22}$
B_{26}	$B^0_{26} - U A^0_{22} + U x_A a^A_{22} + \frac{U^2}{\omega^2} b^A_{22}$
A_{44}	$A^0_{44} - \frac{U}{\omega_e^2} b^A_{44}$
B_{44}	$B^0_{44} + U a^A_{44} + B^*_{44}$
A_{46}	$A^0_{46} + \frac{U}{\omega_e^2} B^0_{24} - \frac{U}{\omega_e^2} x_A b^A_{24} + \frac{U^2}{\omega_e^2} a^A_{24}$
B_{46}	$B^0_{24} - U A^0_{24} + U x_A a^A_{24} + \frac{U^2}{\omega_e^2} b^A_{24}$
A_{62}	$A^0_{62} - \frac{U}{\omega_e^2} B^0_{22} - \frac{U}{\omega_e^2} x_A b^A_{22}$
B_{62}	$B^0_{62} + U A^0_{22} + U x_A a^A_{22}$
A_{64}	$A^0_{64} - \frac{U}{\omega_e^2} B^0_{24} - \frac{U}{\omega_e^2} x_A b^A_{24}$
B_{64}	$B^0_{64} + U A^0_{24} + U x_A a^A_{24}$
A_{66}	$A^0_{66} + \frac{U^2}{\omega_e^2} A^0_{22} - \frac{U}{\omega_e^2} x^2_A b^A_{22} + \frac{U^2}{\omega_e^2} x_A a^A_{22}$
B_{66}	$B^0_{66} + \frac{U^2}{\omega_e^2} B^0_{22} + U x^2_A a^A_{22} + \frac{U^2}{\omega_e^2} x_A b^A_{22}$

References

Abkowitz, M. A. (1964). Lectures on Ship Hydrodynamics - Steering and Maneuverability. Technical Report Hy-5. Hydro- and Aerodynamic's Laboratory. Lyngby, Denmark.

Allensworth, T. (1999). A Short History of Sperry Marine. Internet. <http://www.sperry-marine.com/pages/history.html>.

Bailey, P. A., W. G. Price and P. Temarel (1998). A Unified Mathematical Model Describing the Maneuvering of a Ship Travelling in a Seaway. *Trans. RINA* **140**, 131–149.

Balchen, J. G., N. A. Jenssen and S. Sælid (1976). Dynamic Positioning Using Kalman Filtering and Optimal Control Theory. In: *Proc. of the IFAC/IFIP Symp. On Automation in Offshore Oil Field Operation*. Bergen, Norway. pp. 183–186.

Balchen, J. G., N. A. Jenssen and S. Sælid (1980). Dynamic Positioning of Floating Vessels Based on Kalman Filtering and Optimal Control.. In: *Proceedings of the 19th IEEE Conference on Decision and Control*. New York, NY. pp. 852–864.

Bennet, S. (1979). *A History of Control Engineering 1800-1930*. Peter Peregrinus. London.

Bertram, V. (2004). *Practical Ship Hydrodynamics*. Butterworth-Heinemann. Oxford, UK.

Bishop, R. E. D. and W. G. Price (1981). On the Use of Equilibrium Axes and Body Axis in the Dynamics of a Rigid Ship. *Journal of Mechanical Engineering Science* **IMechE-23**(5), 243–256.

Blanke, M. and A. Christensen (1993). Rudder-Roll Damping Autopilot Robustness due to Sway-Yaw-Roll Couplings. In: *Proc. of the 10th Int. Ship Control Systems Symposium (SCSS'93)*. Ottawa, Canada. pp. A.93–A.119.

Boese, P. (1970). Eine Einfache Methode zur Berechnung der Wiederstandserhöhung eines Schiffes in Seegang. Technical Report Technical Report 258. Institüt für Schiffbau der Universität Hamburg, Germany. in German.

Chislett, M. S. and J. Strøm-Tejsen (1965). Planar Motion Mechanism Tests and Full-Scale Steering and Maneuvering Predictions for a Mariner Class Vessel. Technical Report Hy-6. Hydro- and Aerodynamics Laboratory. Lyngby, Denmark.

Clarke, D. (2003). The Foundations of Steering and Maneuvering. In: *Proc. of the IFAC Conf. on Control Applications in Marine Systems (CAMS'03)*. Girona, Spain. Plenary Talk.

Cummins, W. E. (1962). The Impulse Response Function and Ship Motions. Technical Report 1661. David Taylor Model Basin. Hydromechanics Laboratory, USA.

Denis, M. St. and W. J. Pierson (1953). On the Motions of Ships in Confused Seas. *Trans. SNAME* **61**, 280–357.

Faltinsen, O. M. (1990). *Sea Loads on Ships and Offshore Structures*. Cambridge University Press.

Faltinsen, O. M. and R. Zhao (1991*a*). Flow Predictions Around High-Speed Ships in Waves. In: *Mathematical Approaches in Hydrodynamics, SIAM*. pp. 1–27.

Faltinsen, O. M. and R. Zhao (1991*b*). Numerical Predictions of Ship Motions at High Forward Speed. In: *Philosophical Transaction of the Royal Society, Series A*. pp. 241–252.

Faltinsen, O. M. and T. Svensen (1990). Incorporation of Seakeeping Theories in CAD. International Symposium on CFD and CAD in Ship Design, MARIN, Wageningen, The Netherlands.

Fathi, D. (2004). ShipX Vessel Responses (VERES). Marintek AS, Trondheim.

Fathi, D. and J. R. Hoff (2004). ShipX Vessel Responses (VERES). Theory Manual, Marintek AS.

Fedyaevsky, K. K. and G. V. Sobolev (1963). Control and Stability in Ship Design. State Union Shipbuilding Publishing House, Leningrad.

Fossen, T. I. (1994). *Guidance and Control of Ocean Vehicles*. John Wiley and Sons Ltd. ISBN 0-471-94113-1.

Fossen, T. I. (2002). *Marine Control Systems: Guidance, Navigation and Control of Ships, Rigs and Underwater Vehicles*. Marine Cybernetics AS. Trondheim, Norway. ISBN 82-92356-00-2.

Fossen, T. I. and J. P. Strand (1999). Passive Nonlinear Observer Design for Ships Using Lyapunov Methods: Experimental Results with a Supply Vessel. *Automatica* **AUT-35**(1), 3–16.

Fossen, T. I. and Ø. Smogeli (2004). Nonlinear Time-Domain Strip Theory Formulation for Low-Speed Maneuvering and Station-Keeping. *Modelling, Identification and Control* **MIC-25(4)**, 201–221.

Frank, W. (1967). Oscillation of Cylinders in or below the Free Surface of Deep Fluids. Technical Report Technical Report 2375. Naval Ship Research and Development Centre, Washington DC, U.S.A.

Gerritsma, J. (1960). Ship Motions in Longitudinal Waves. *International Shipbuilding Progress* **ISP-7**, 49–76.

Gerritsma, J. and W. Beukelman (1972). Analysis of the Resistance Increase in Waves of a Fast Cargo-Ship. *International Shipbuilding Progress*.

Gertler, M. (1959). The DTMB Planar Motion Mechanism System. In: *Proceedings of Symposium on Towing Tank Facilities, Instrumentation and Measuring Techniques*. Zagreb, Yugoslavia.

Grim, O. (1953). Berechnung der durch Schwingungen eines Schiffskörpers Erzeugten Hydrodynamischen Kräfte. *Jahrbuch der Schiffsbautechnischen Gesellschaft* **47**, 277–299. in German.

Grimble, M. J., R. J. Patton and D. A. Wise (1979). The Design of Dynamic Positioning Systems using Extended Kalman Filtering Techniques. In: *Proceedings of OCEANS'79*. pp. 488–497.

Grimble, M. J., R. J. Patton and D. A. Wise (1980). The Design of Dynamic Positioning Control Systems Using Stochastic Optimal Control Theory. *Optimal Control Applications and Methods* **OCAM-1**, 167–202.

Ikeda, Y., Y. Himeno and N. Tanaka (1978). A Prediction Method for Ship Rolling. Technical Report 00405. Department of Naval Architecture, University of Osaka Prefecture, Japan.

Journée, J.M.J. and W.W. Massie (2001). *Offshore Hydromechanics*. Delft University of Technology. The Netherlands.

Katebi, M. R., M. J. Grimble and Y. Zhang (1997). H_∞ Robust Control Design for Dynamic Ship Positioning. In: *IEE Proceedings on Control Theory and Applications*. Vol. 144 2. pp. 110–120.

Keil, H. (1974). Die Hydrodynamische Kräfte bei der periodischen Bewegung zweidimensionaler Körper an der Oberfläche flacher Gewasser. Technical Report 305. Institut für Schiffbau der Universität Hamburg, Deutschland.

Korsmeyer, F. T., H. B. Bingham and J. N. Newman (1999). TiMIT - A Panel Method for Transient Wave-Body Interactions. Research Laboratory of Electronics, MIT.

Korvin-Kroukovsky, B. V. and W. R. Jacobs (1957). Pitching and Heaving Motions of a Ship in Regular Waves. *Transactions SNAME* **65**, 590–632.

Kristiansen, E. (2005). State Space Representation of Hydrodynamic Memory Effects. PhD thesis. Dept. of Eng. Cybernetics, Norwegian University of Science and Technology.

Kristiansen, E. and O. Egeland (2003). Frequency-Dependent Added Mass in Models for Controller Design for Wave Motion Damping. In: *IFAC Conference on Maneuvering and Control of Marine Systems (MCMC'03)*. Girona, Spain.

Lewis, E. V., Ed.) (1989). *Principles of Naval Architecture*. 2nd ed.. Society of Naval Architects and Marine Engineers (SNAME).

Minorsky, N. (1922). Directional Stability of Automatic Steered Bodies. *J. Amer. Soc. of Naval engineers* **34**(2), 280–309.

MSS (2004). Marine Systems Simulator. Norwegian University of Science and Technology, Trondheim <www.cesos.ntnu.no/mss>.

Newman, J. N. (1977). *Marine Hydrodynamics*. MIT Press. Cambridge, MA.

Nomoto, K., T. Taguchi, K. Honda and S. Hirano (1957). On the Steering Qualities of Ships. Technical report. International Shipbuilding Progress, Vol. 4.

Norrbin, N. H. (1963). On the Design and Analyses of the Zig-Zag Test on Base of Quasi Linear Frequency Response. Technical Report B 104-3. The Swedish State Shipbuilding Experimental Tank (SSPA). Gothenburg, Sweden.

Norrbin, N. H. (1970). Theory and Observation on the use of a Mathematical Model for Ship Maneuvering in Deep and Confined Waters. In: *Proc. of the 8th Symposium on Naval Hydrodynamics*. Pasadena, California. pp. 807–904.

Ogilvie, T. F. (1964). Recent Progress towards the Understanding and Prediction of Ship Motions. In: *5th Symposium on Naval Hydrodynamics*. pp. 3–79.

Perez, T. (2005). *Ship Motion Control: Autopilots with Rudder Roll Stabilization and Combined Rudder-Fin Stabilizators*. Springer-Verlag. Advances in Industrial Control Series.

Perez, T. and T. I. Fossen (2004). A Discussion about Seakeeping and Maneuvering Models for Surface Vessels. Technical Report MSS-TR-001. Marine System Simulator, Norwegian University of Science and Technology.

Salvesen, N., E. O. Tuck and O. M. Faltinsen (1970). *Ship Motions and Sea Loads*. Trans. SNAME, vol. 78, pp. 250–287.

SNAME (1950). The Society of Naval Architects and Marine Engineers. Nomenclature for Treating the Motion of a Submerged Body Through a Fluid. In: *Technical and Research Bulletin No. 1-5*.

Sørensen, A. J. (2005). Structural Properties in the Design and Operation of Marine Control Systems. *IFAC Journal on Annual Reviews in Control*.

Sørensen, A. J., S. I. Sagatun and T. I. Fossen (1995). The Design of a Dynamic Positioning System Using Model Based Control. In: *Proceedings of the IFAC Workshop on Control Applications in Marine Systems (CAMS'95)*. Trondheim, Norway. pp. 16–26.

Tasai, F. (1959). On the Damping Force and Added Mass of Ships Heaving and Pitching. Technical Report 26. Technical Report, Research Institute for Applied Mechanics, Kyushu University. Japan.

Tasai, F. (1960). Formula for Calculating Hydrodynamic Force on a Cylinder Heaving in the Free Surface, (N-Parameter Family). Technical Report 31. Technical Report, Research Institute for Applied Mechanics, Kyushu University. Japan.

Tasai, F. (1961). Hydrodynamic Force and Moment Produced by Swaying and Rolling Oscillation of Cylinders on the Free Surface. Technical Report 35. Technical Report, Research Institute for Applied Mechanics, Kyushu University. Japan.

Ursell, F. (1949). On the Heaving Motion of a Circular Cylinder on the Surface of a Fluid. *Quarterly Journal of Mechanics and Applied Mathematics*.

WAMIT (2004). User manual. <www.wamit.com>. WAMIT, Inc. 822 Boylston St. Suite 202 Chestnut Hill, MA 02467-2504 USA.